Chemical Science

ROYAL SOCIETY OF CHEMISTRY

PERSPECTIVE

View Article Online
View Journal | View Issue

Check for updates

Cite this: *Chem. Sci.*, 2023, **14**, 5827

All publication charges for this article have been paid for by the Royal Society of Chemistry

Received 27th February 2023
Accepted 10th May 2023

DOI: 10.1039/d3sc01088k

rsc.li/chemical-science

Lanthanide molecular cluster-aggregates as the next generation of optical materials

Diogo Alves Gálico, Claudia Manuela Santos Calado and Muralee Murugesu *

In this perspective, we provide an overview of the recent achievements in luminescent lanthanide-based molecular cluster-aggregates (MCAs) and illustrate why MCAs can be seen as the next generation of highly efficient optical materials. MCAs are high nuclearity compounds composed of rigid multinuclear metal cores encapsulated by organic ligands. The combination of high nuclearity and molecular structure makes MCAs an ideal class of compounds that can unify the properties of traditional nanoparticles and small molecules. By bridging the gap between both domains, MCAs intrinsically retain unique features with tremendous impacts on their optical properties. Although homometallic luminescent MCAs have been extensively studied since the late 1990s, it was only recently that heterometallic luminescent MCAs were pioneered as tunable luminescent materials. These heterometallic systems have shown tremendous impacts in areas such as anti-counterfeiting materials, luminescent thermometry, and molecular upconversion, thus representing a new generation of lanthanide-based optical materials.

Open Access Article. Published on 10 2023. Downloaded on 2024/9/11 7:21:17.
This article is licensed under a Creative Commons Attribution-NonCommercial 3.0 Unported Licence.

1. Introduction

Over the past few decades, the study of luminescent materials based on trivalent and divalent lanthanide ions has garnered much attention, with successful applications in diverse fields such as lighting, bioimaging, and the development of luminescent probes for temperature, ions, pH, pressure, and other analytes.[1–35] Despite numerous reports published in this field, it remains an effervescent research topic with new developments reported frequently, including new applications and/or improved performance.

Although not restricted to nanoparticles[36–40] and molecular complexes,[41–45] both classes of materials represent the most studied systems for optical applications, each with its own merits and limitations. For example, much of the success in using nanoparticles relies on fine tunability of the composition due to the large number of metal ions within the crystalline lattice, enabling optimization of the optical properties through precise control of composition, with the main drawback still being the lack of homogeneity with size distribution. As a result, the observed property attained will be the result of different smaller parts. On the other hand, molecular compounds offer atomic-level control due to their well-defined structure. However, the limited number of metal ions in such compounds restricts the effectiveness of energy-transfer (ET) processes between different lanthanides, thereby limiting the possibilities for controlling optical output.

Department of Chemistry and Biomolecular Sciences, University of Ottawa, Ottawa, Ontario K1N 6N5, Canada. E-mail: m.murugesu@uottawa.ca

In this perspective, we will highlight an emerging class of lanthanide materials, molecular cluster-aggregates (MCAs), for their optical applications. We will discuss the advantages of this class of materials in terms of composition, ET, and control over their optical output. Our focus will be on recent achievements in the luminescence of trivalent lanthanide-based MCAs. Furthermore, we will not delve into the synthetic strategies[46–50] or the theoretical aspects of lanthanides luminescence[51–55] but rather we summarize and highlight some of the recent achievements in this area.

This article starts with a brief discussion about lanthanide-based MCAs (Section 2) and trivalent lanthanide luminescence (Section 3). We subsequently focused our attention on homometallic luminescent MCAs (Section 4) before discussing the impacts and potential that heterometallic MCAs could have in some applications which require effective control of ET processes, such as luminescent thermometers and anti-counterfeiting materials (Section 5). We conclude this perspective by providing an outlook on possible future directions and their potential implications for the field of optical materials.

2. Lanthanide-based molecular cluster-aggregates

Lanthanide-based MCAs are composed of rigid multinuclear metal cores encapsulated by organic ligands.[46–50,56–73] These systems are arranged in a highly ordered structure in a crystal lattice, presenting a high uniformity due to the molecular origin. The nuclearity of MCAs can range from a few to

© 2023 The Author(s). Published by the Royal Society of Chemistry

Open Access Article. Published on 10 2023. Downloaded on 2024/9/11 7:21:17.
This article is licensed under a Creative Commons Attribution-NonCommercial 3.0 Unported Licence.

hundreds of metal ions (Fig. 1), with larger ones comparable to the ultrasmall nanoparticles in size.[74–78] In the late 90s, lanthanide-based MCAs gained attention due to their aesthetic beauty, remarkable physical properties such as luminescence and magnetism, as well as the synthetic challenge of producing large nuclearity systems.

For the latter, Staples, Zheng, and co-workers paved the way in the study of the synthetic coordination chemistry of lanthanides at high pH by pioneering the control of hydrolysis and halide-templating in a pentadecanuclear lanthanide system.[84–86] This resulted in new strategies for producing high-nuclearity MCAs with a certain degree of control. Since then, several research groups have successfully reported intriguing and impressive giant complexes such as **{Er$_{60}$}**,[82,87–90] **{Nd$_{104}$}**,[91] and **{Gd$_{140}$}**,[83] mostly being developed by Long, Zheng, Kong and co-workers.

Structurally, MCAs can be viewed as a merging of the nanoparticle and molecular complex realms (Scheme 1). The sizes and high nuclearities resemble those observed for ultrasmall nanoparticles while maintaining high homogeneity in size and number of metal ions due to the molecular nature. Therefore, achieving high performance and fine-tunability in the composition akin to nanoparticles is possible while alleviating issues related to size distribution.

From the application perspective, earlier high-nuclearity MCAs were primarily designed for use as molecular magnetic coolers.[62–70] Little attention was paid to exploring their potential as highly efficient optical materials. However, in recent years, our research group has been focused on developing heterometallic MCAs for various applications, unlocking the vast potential of this class of compounds.[79,81,92–96]

3. Luminescence of trivalent lanthanides

Lanthanides ions are well known for their remarkable and versatile luminescent properties. In this perspective article, a detailed discussion of lanthanide luminescence theory is out of our scope. For this topic, readers can find specialized and detailed reviews.[51–55] We intend to marginally describe some essential features that will appear in examples discussed in Sections 4 and 5. Except for Ce^{3+} and some divalent lanthanide ions (such as Eu^{2+} and Yb^{2+}), the typical luminescence observed for most trivalent lanthanide ions (Ln^{3+}) originates from electronic transitions within the partially filled $4f^n$ orbitals. An essential feature of lanthanides is the shielded nature of the 4f orbitals by the $5s^25p^6$ subshells, thus resulting in an inner orbital character. This remarkable feature is responsible for the unique optical properties of the lanthanides and results in particularly sharp absorption and emission lines characteristic of each lanthanide. In terms of energetic position, the 4f–4f transitions are thus little sensitive to the external environment and have a fingerprint for different lanthanide ions. The characteristic emissions of the Ln^{3+} ions span from the ultraviolet-(UV) to the near-(NIR) and mid-infrared range of the electromagnetic spectrum, according to the individual ladder-like structure (Fig. 2) and are characterized by relatively long lifetimes (in the order of micro to milliseconds).

Another crucial aspect of the 4f–4f transitions is the parity-forbidden nature of these transitions. Laporte's rule forbids intraconfigurational electric dipole transitions, such as 4f–4f.[97] Consequently, due to the low transition probabilities, the absorption cross-sections for lanthanide ions are much smaller than other luminescent species. Hence, the relaxation of the

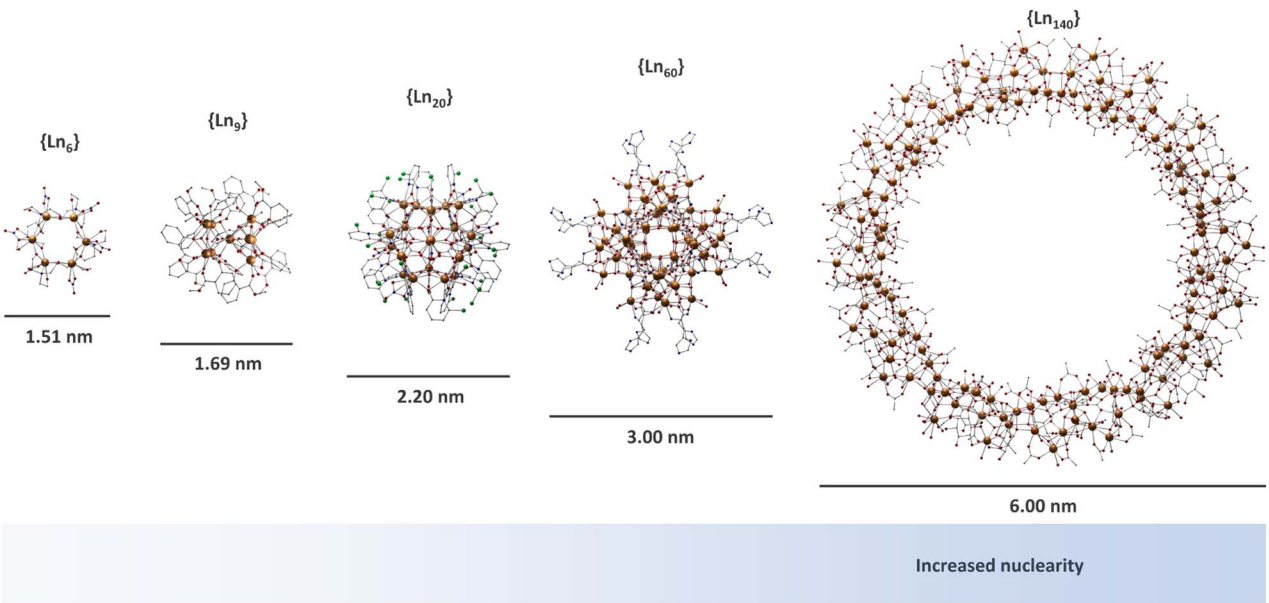

Fig. 1 Molecular structure of selected MCAs. **{Ln$_6$}** (CCDC number: 1958091);[79] **{Ln$_9$}** (CCDC number: 956639);[80] **{Ln$_{20}$}** (CCDC number: 2023766);[81] **{Ln$_{60}$}** (CCDC number: 2152485);[82] and **{Ln$_{140}$}** (CCDC number: 1569507).[83] Colour code: Dark orange: Ln^{3+}; grey: carbon; red: oxygen; blue: nitrogen; light green: chlorine. Hydrogen atoms were omitted in all structures for clarity.

© 2023 The Author(s). Published by the Royal Society of Chemistry

Open Access Article. Published on 10 2023. Downloaded on 2024/9/11 7:21:17.
This article is licensed under a Creative Commons Attribution-NonCommercial 3.0 Unported Licence.

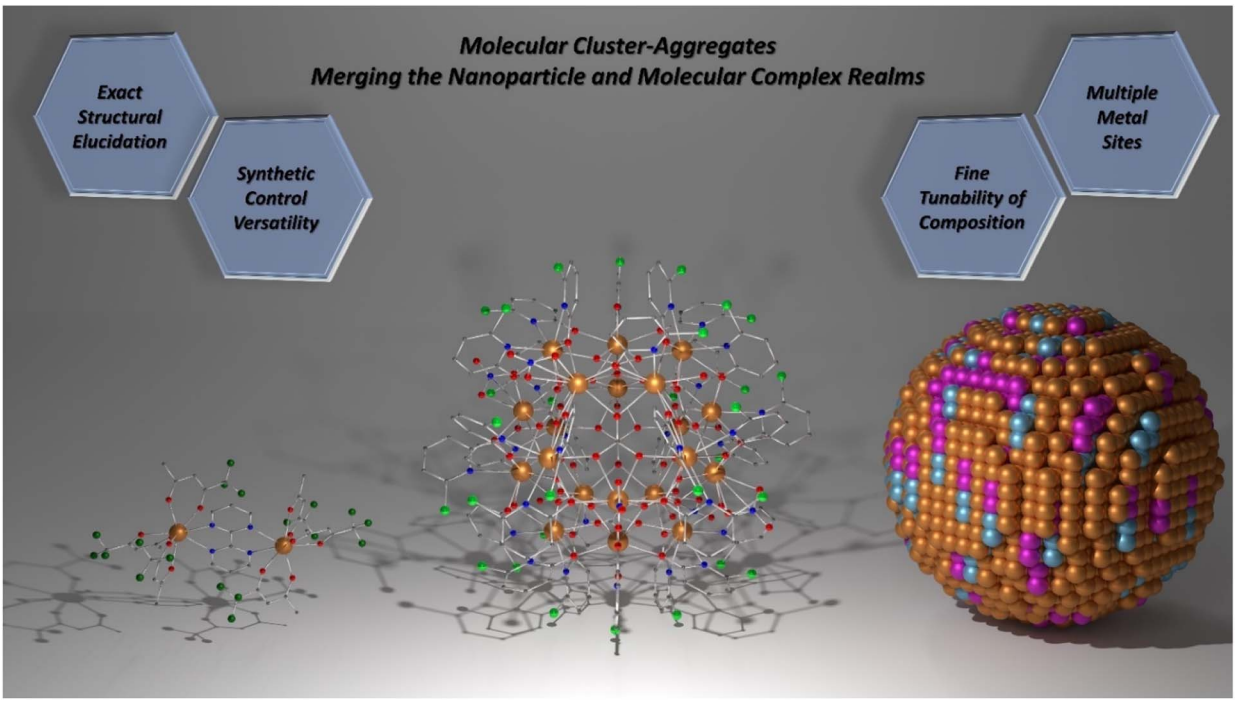

Scheme 1 Molecular cluster-aggregates. The union between molecular complex and nanoparticle worlds. Left: $[Dy_2(bpm)(tfaa)_6]$ complex (CCDC number: 1859276).[98] Centre: **{Eu_{20}}** MCA (CCDC number: 2023766).[81] Right: Representation of a heterometallic spherical nanoparticle. Colour code for left and centre: dark orange: Ln^{3+}; grey: carbon; red: oxygen; blue: nitrogen; light green: chlorine; dark green: fluoride. Hydrogen atoms were omitted in all structures for clarity. For the nanoparticle representation, colours were randomly chosen and have no meaning.

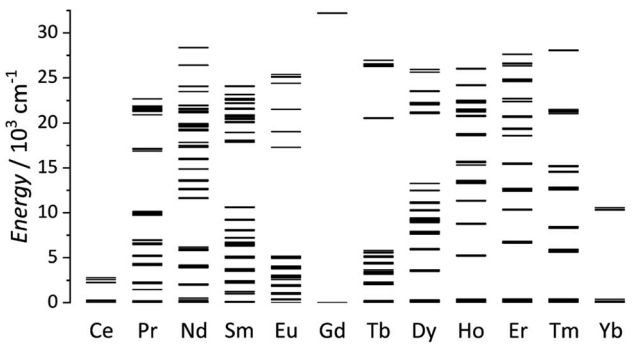

Fig. 2 Partial energy-levels diagram for trivalent lanthanides. Energies obtained from Carnall.[99]

selection rules is pivotal for making the 4f–4f transitions "less forbidden".

This can be achieved by placing the lanthanide ion in a non-centrosymmetric coordination environment, resulting in mixing electronic and vibrational wavefunctions. Even though the wavefunctions mixing makes the 4f–4f transitions less forbidden, transition probabilities remain weak with molar absorption coefficients much smaller than 100 M^{-1} cm^{-1}.

Considering this, some strategies have been developed to effectively harvest the energy to the emitter levels of each lanthanide. Some of the approaches relevant to understanding the examples in Sections 4 and 5 will be briefly discussed here.

When Ln^{3+} ions are placed in close proximity to each other, ET processes could be efficiently controlled to modulate the optical output.[100–108] This is an easy task for nanoparticles, with hundreds to tens of thousands of metal ions, but more limited for low nuclearity molecular complexes. Since efficient ET transfer is at the crux of the upconversion (UC) mechanism (*vide infra*),[109–112] it is easy to understand the supremacy of nanoparticles over molecular UC.

3.1 Antenna effect

The antenna effect, also known as ligand-mediated intramolecular ET, was first demonstrated in the seminal studies of Weissman and Crosby.[113–115] This strategy relies on using an organic compound, which usually has a much larger absorption cross-section to absorb light and transfer it to Ln^{3+} ions (Fig. 3). Briefly, the ligand absorbs the light, populating the excited singlet states (S_n). An intersystem crossing (ISC) occurs, thus populating the ligand triplet state (T). Subsequently, the energy is transferred to the Ln^{3+} excited states that can radiatively emit *via* the individually characteristic 4f–4f transitions. From the ligand side, two critical conditions are required for an efficient ligand-to-Ln^{3+} ET to occur:

(1) An efficient ISC process: For this, an energy gap of at least 5000 cm^{-1} between the ligand S_1 and T_1 is required.[116–118]

(2) An efficient T_1 to Ln^{3+} ET process: According to Latva's empirical rules, the optimal gap between the ligand T_1 state and Ln^{3+} emitter level is around 2500–4000 cm^{-1}. Energetic

Open Access Article. Published on 10 2023. Downloaded on 2024/9/11 7:21:17.
This article is licensed under a Creative Commons Attribution-NonCommercial 3.0 Unported Licence.

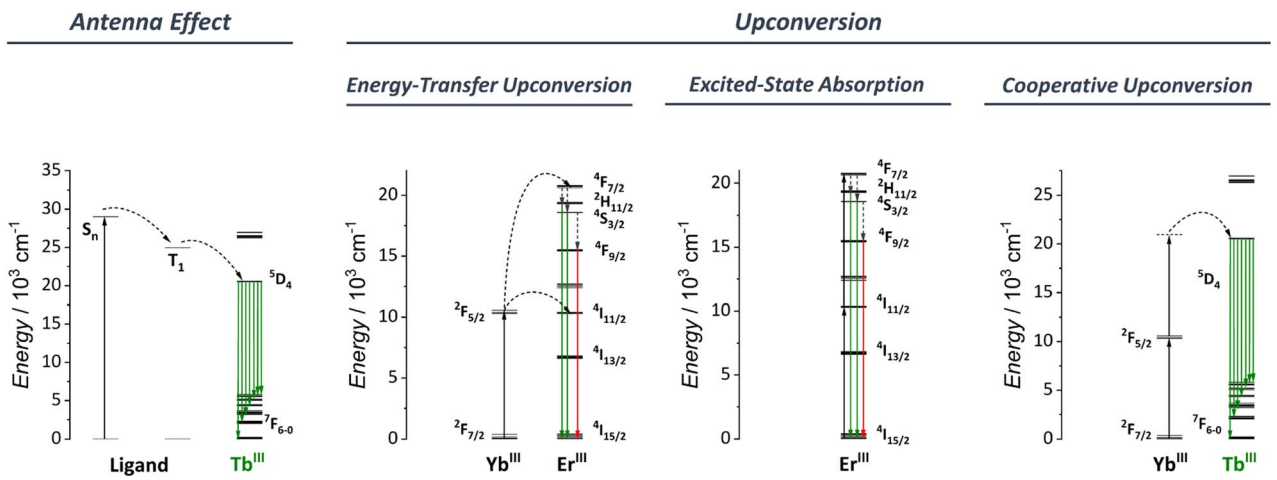

Fig. 3 Depiction of some commonly observed luminescence mechanisms for Ln^{3+} ions. From left to right: Ligand-based antenna effect, Yb^{3+}-Er^{3+}-based energy-transfer upconversion, Er^{3+}-based excited-state absorption, and Yb^{3+}-Tb^{3+}-based cooperative upconversion.

differences above 4000 cm^{-1} do not allow an efficient ET. Energetic differences below 2500 cm^{-1} result in a strong back energy-transfer (BET) from the Ln^{3+} ion to the ligand.[119]

3.2 Upconversion

Upconversion (UC) is an intriguing phenomenon involving the sequential absorption of two or more low-energy photons resulting in the emission of higher-energy photons. Unlike the nonlinear optics processes such as second-harmonic generation, UC is based on the cumulative effects of multiple first-order absorption processes such as excited-state absorption (ESA), energy transfer upconversion (ETU), and cooperative upconversion (CUC), showing a higher efficiency than the nonlinear processes.

Bloembergen first observed the phenomenon of upconversion in 1959,[120] but it wasn't until the pioneering research of Auzel,[121] Ovsyankin, and Feofilov[122] in 1966 that an appropriate understanding and explanation was developed. Since then, UC has been extensively studied in low-phonon solid materials and nanoparticles, with applications in a variety of fields, including bioimaging,[123–128] photodynamic therapy,[129–133] optogenetics,[134–138] upconversion lasing,[139–143] super-resolution microscopy,[144–148] luminescence thermometry,[149–158] anti-counterfeiting materials,[159–163] and many others.

Fig. 3 shows a simplified diagram for some of the UC mechanisms relevant to the discussion in Section 5. This perspective does not focus on reviewing the different UC mechanisms. For this, we recommend that readers to consider the review article by Auzel.[109]

Until the early 2000s, studies of the upconversion phenomena were mainly focused on Ln^{3+}-based nanoparticles and low-phonon solid materials. Since then, some groups have started investigating the UC process in low-nuclearity molecular compounds to overcome some intrinsic issues inherent to nanoparticles (*vide supra*). Despite the success of the earlier works in observing UC in molecular species, the use of low-nuclearities compounds resulted in low upconversion quantum yields (UCQY),[164–170] much below the values observed for nanoparticles and low-phonon solid materials.[171–173]

3.3 Why luminescent MCAs?

As mentioned in Section 2, MCAs represent the union of two of the most explored classes of lanthanide materials for luminescence, nanoparticles and molecular complexes. As such, the benefits of both classes can be attained in a single unit by using MCAs. Due to the chemical similarities, it is possible to replace one lanthanide with another within these molecular entities, thus, modifying the chemical composition, and consequently, the ET processes as seen for NPs.[100–108] However, at the same time, the molecular nature allows for the precise determination of the lanthanide local symmetry/distortions, which is not entirely possible and understood through the huge surface metal sites in nanoparticles. Consequently, higher uniformity/homogeneity in the optical properties is expected for different synthetic batches of MCAs and at an individual level. Additionally, the presence of organic ligands as a constituent part of the MCA structure makes it possible for an efficient antenna effect without needing surface modification.

4. Optical properties of homometallic MCAs

The study of luminescent homometallic MCAs dates to the late 90s and early 2000s. The first reported example is related to a pentanuclear europium MCA assembled *via* a ligand-controlled hydrolysis using dibenzoylmethane (Hdbm) as the ligand.[174] In this work, the Eu^{3+} ion luminescence was used only as a structural probe to confirm the observations that all five Eu^{3+} ions possess the exact local symmetry. Since then, several examples of luminescent homometallic with the most diverse nuclearities have been reported (Table 1). Most of these works report the presence of luminescence on the MCAs; however, some are important in understanding the potential of lanthanide-based MCAs as luminescent materials and will be

© 2023 The Author(s). Published by the Royal Society of Chemistry

Open Access Article. Published on 10 2023. Downloaded on 2024/9/11 7:21:17.
This article is licensed under a Creative Commons Attribution-NonCommercial 3.0 Unported Licence.

Table 1 Summary of homometallic luminescent MCAs[a]

	Capping ligand	Emitter ion	Lifetime/μs	Quantum yield/%	Reference
$\{Ln_5\}$	Dibenzoylmethane	Eu^{3+}	0.06	—	174
$\{Ln_5\}$	Dibenzoylmethane	Eu^{3+}	—	—	183
$\{Ln_5\}$	Dibenzoylmethane	Tb^{3+}	—	—	183
$\{Ln_5\}$	Dibenzoylmethane	Nd^{3+}	8.29	—	184
$\{Ln_5\}$	Dibenzoylmethane	Yb^{3+}	9.95	—	184
$\{Ln_6\}$	Triethanolamine	Er^{3+}	—	—	79
$\{Ln_8\}$	2,2,6,6-Tetramethylheptane-3,5-dione	Eu^{3+}	—	—	183
$\{Ln_8\}$	2,2,6,6-Tetramethylheptane-3,5-dione	Tb^{3+}	—	—	183
$\{Ln_9\}$	Benzoylacetone	Eu^{3+}	—	—	176
$\{Ln_9Na_{10}\}$	5′-Methyl-2,2′-bipyridyl-6-phosphonic acid	Eu^{3+}	2370, 240	32	185
$\{Ln_9Na_{10}\}$	5′-Methyl-2,2′-bipyridyl-6-phosphonic acid	Yb^{3+}	9.3	0.22	185
$\{Ln_9\}$	Hexylsalycilate	Tb^{3+}	1200	90	179
$\{Ln_9\}$	Hexylsalycilate	Yb^{3+}	2, 0.6	—	179
$\{Ln_9\}$	Acetylacetonate	Eu^{3+}	—	—	183
$\{Ln_9\}$	Acetylacetonate	Tb^{3+}	—	—	183
$\{Y_{9-n}Ln_n\}$	Acetylacetonate	Eu^{3+}	—	—	186
$\{Ln_9\}$	2-(Hydroxymethyl)pyridine	Eu^{3+}	—	—	187
$\{Ln_9\}$	Methyl 4-methylsalicylate	Tb^{3+}	815	31	180
$\{Ln_9\}$	Methyl 5-methylsalicylate	Tb^{3+}	190	2.4	180
$\{Ln_9\}$	Methylsalicylate	Tb^{3+}	264	6.7	180
$\{Ln_1Gd_8\}$	Butylsalicylate	Tb^{3+}	960	14	188
$\{Ln_2Gd_7\}$	Butylsalicylate	Tb^{3+}	1060	23	188
$\{Ln_5Gd_4\}$	Butylsalicylate	Tb^{3+}	1160	33	188
$\{Ln_8Gd_1\}$	Butylsalicylate	Tb^{3+}	1170	40	188
$\{Ln_9\}$	Butylsalicylate	Tb^{3+}	1160	39	188
$\{Ln_1Gd_8\}$	Butylsalicylate	Yb^{3+}	0.57	—	189
$\{Ln_3Gd_6\}$	Butylsalicylate	Yb^{3+}	0.56	—	189
$\{Ln_7Gd_2\}$	Butylsalicylate	Yb^{3+}	0.57	—	189
$\{Ln_1Lu_8\}$	Butylsalicylate	Yb^{3+}	0. 74	—	189
$\{Ln_3Lu_6\}$	Butylsalicylate	Yb^{3+}	0.63	—	189
$\{Ln_7Lu_2\}$	Butylsalicylate	Yb^{3+}	0.61	—	189
$\{Ln_9\}$	Butylsalicylate	Yb^{3+}	0.60	—	189
$\{Ln_{13}\}$	$(Ph_4Si_4O_8)^{4-}$	Eu^{3+}	884	50	181
$\{Ln_{14}\}$	Acetylacetonate	Tb^{3+}	—	—	190
$\{Ln_{14}\}$	Acetylacetonate	Dy^{3+}	—	—	190
$\{Ln_{14}\}$	2,3-Dihydroxybenzaldehyde	Yb^{3+}	7.83	0.24	191
$\{Ln_{14}\}$	2,3-Dihydroxybenzaldehyde	Nd^{3+}			192
$\{Ln_{15}\}$	$PepCO_2$ and dibenzoylmethane	Eu^{3+}	—	16	182
$\{Ln_{15}\}$	$PepCO_2$ and dibenzoylmethane	Tb^{3+}	—	<3	182
$\{Ln_{18}\}$	L_1 and 2,3-dihydroxybenzaldehyde	Yb^{3+}	9.11	0.16	193
$\{Ln_{18}\}$	L_1 and 2,3-dihydroxybenzaldehyde	Nd^{3+}	6.44	0.17	194
$\{Ln_{18}\}$	L_1 and 2,3-dihydroxybenzaldehyde	Eu^{3+}	—	—	195
$\{Ln_{20}\}$	3,5-Bis[3-(pyrid-2-yl)-1,2,4-triazolyl]-pyridine	Tb^{3+}	605	—	196
$\{Ln_{20}\}$	Chloro-2-pyridinol	Eu^{3+}	—	—	81
$\{Ln_{20}\}$	Chloro-2-pyridinol	Tb^{3+}	1314, 454, 107	55.8	81
$\{Ln_{42}\}$	2-Hydroxy-3-methoxybenzaldehyde	Nd^{3+}	6.37	0.76	197
$\{Ln_{42}\}$	2-Hydroxy-3-methoxybenzaldehyde	Yb^{3+}	11.65	0.20	198
$\{Ln_{42}\}$	2-Hydroxy-3-methoxybenzaldehyde	Sm^{3+}	15.65	0.33	198
$\{Ln_{42}\}$	2-Hydroxy-3-methoxybenzaldehyde	Eu^{3+}	22.8	1.74	199
$\{Ln_{42}\}$	2-Hydroxy-3-methoxybenzaldehyde	Tb^{3+}	—	<0.1	199
$\{Ln_{48}\}$	2-Thiophenecarboxylic acid	Eu^{3+}	284	8.40	200
$\{Ln_{48}\}$	3-Furancarboxylic acid	Tb^{3+}	905	3.11	200

[a] $PepCO_2$ = 2-[{3-(((*tert*-butoxycarbonyl)amino)methyl)benzyl}amino]acetic acid. L_1 = 3,3′-((1*E*,1′*E*)-((4,5-dimethyl-1,2-phnylene)bis(azaneylylidene))bis(methaneylylidene))bis(benzene-1,2-diol).

discussed in this section. It should be noted that homometallic MCAs as luminescent materials are less attractive in application potential, as almost no differences will be observed compared to low-nuclearity molecular complexes. All the attractiveness of using MCAs as luminescent materials relies on the possibility of controlling the composition and ET processes (see next section).

In 2020, our group reported the first demonstration of NIR-to-NIR emission on a water-soluble Er^{3+}-based MCA.[79] The $[Er_6(teaH)_6(NO_3)_6]$ exhibit a wheel-like molecular structure in which each Er^{3+} is encapsulated by one $teaH^{2-}$ (doubly

Open Access Article. Published on 10 2023. Downloaded on 2024/9/11 7:21:17.
This article is licensed under a Creative Commons Attribution-NonCommercial 3.0 Unported Licence.

deprotonated triethanolamine) and one nitrate anion. We demonstrated the water stability *via* NMR of the Y^{3+} analogue and by TGA, powder X-ray, and FTIR analysis of the **{Er$_6$}** MCA powder before and after a solubilization/drying procedure. By exciting the MCA with a 980 nm laser, we observed the characteristic telecom range $^4I_{13/2} \rightarrow {}^4I_{15/2}$ transition band centred at approximately 1530 nm. This was an exciting result as NIR-to-NIR emissions are critical for biomedical imaging, telecommunications, photonics and optoelectronics fields.[175]

Among all the possible nuclearities, nonanuclear hourglass-like MCAs are the most studied in luminescence. These robust systems can be seen as two square pyramids sharing the apical vertex (Fig. 4) and are easily synthesized, stable in several solvents, and the most attractive fact is that they can be prepared with different encapsulating ligands, promoting a toolbox to investigate the impact of other organic moieties on the MCAs luminescent properties.

The first luminescent nonanuclear MCA was reported by Yan and co-workers in 2002.[176] These MCAs, $[Ln_9(\mu_4\text{-}O)_2(\mu_3\text{-}OH)_8(\mu\text{-}BA)_8(BA)_8]^-[HN(CH_2CH_3)_3]^+\cdot(CH_3OH)_2(CHCl_3)$ (Ln = Sm^{3+}, Eu^{3+}, Gd^{3+}, Dy^{3+}, and Er^{3+}) were assembled using benzoylacetone (BA) as the ligand. However, luminescent properties were reported only for the **{Eu$_9$}** congener. This outcome is not surprising, as the triplet state of BA is positioned at around 21 700 cm^{-1},[177,178] which makes it an ideal energetic position to sensitize Eu^{3+} ions, but not others.

On the other hand, in 2007, Kushida and co-workers reported Tb^{3+} and Yb^{3+} homometallic **{Ln$_9$}** MCAs with the same metal core topology with hexylsalicylate as the capping ligand.[179] The triplet state of this ligand is located approximately at 23 200 cm^{-1}, 2800 cm^{-1} above the Tb^{3+} $^5D_4$ emitter level, thus, acting as a highly efficient antenna for Tb^{3+} sensitization. Consequently, an impressive emission quantum yield of 90% was observed. For the **{Yb$_9$}** analogue, the NIR emission was observed but too weak to allow a complete study.

Posteriorly, Hasegawa and co-workers published a report describing the same nonanuclear core-structure surrounded by methylsalycilate, methyl 4-methylsalicylate, and methyl 5-methylsalicylate.[180] The triplet state of these ligands occurs at lower energies than the previous example (hexylsalicylate) and the energetic proximity of the triplet state and Tb^{3+} emitter level results in a more pronounced back-ET, and consequently, lower quantum yields.

These previous works show the elegance of the nonanuclear hourglass-like MCAs. By changing the capping ligand, while keeping the same metal-core structure, the first system is optimal for sensitizing Eu^{3+} while the second one acts as a better sensitizer for Tb^{3+} ions. The study of luminescent homometallic **{Ln$_9$}** MCAs were further extended for systems containing several other ligands (Table 1).

In 2022, Sun and co-workers reported a **{Eu$_{13}$}** nanocage exhibiting a Keggin-like structure, prepared with a highly symmetric $(Ph_4Si_4O_8)^{4-}$ capping ligand.[181] This MCA has a similar fourfold symmetry as that of the macrocyclic tetrasilane and shows potential for application in optical, catalysis, and photoelectric fields. The rigid structure in which the Eu^{3+} atoms are bridged by O^{2-} rather than the OH^- bridges commonly observed for MCAs results in a higher quantum yield (50%) due to the reduced vibrational quenching pathways.

In 2013, Roesky and co-workers described a pentadecanuclear system as the first MCA prepared with peptoids as supporting ligands for nanoscale bio-compatible applications.[182] The $[Ln_{15}(\mu_3\text{-}OH)_{20}(PepCO_2)_{10}(DBM)_{10}Cl]^{4+}$ MCA is assembled *via* heterocubane subunits organized in a pentagonal ring arrangement. The photoluminescence studies of Eu^{3+} and Tb^{3+}-based systems showed the expected emission in the visible range, and their applicability as probes in cell culture was evaluated using time-resolved luminescent microscopy. *In vitro* studies with HeLa tumour cells revealed an accumulation of the clusters in the endosomal-lysosomal system with moderate cytotoxicity for these cells.

Recently, our group started studying one of the most versatile MCA for optical applications, **{Ln$_{20}$}**.[81] This icosanuclear MCA consists of a rigid spherical metal-core surrounded by chloro-2-pyridinol (chp) ligands with the $[Ln_{20}(chp)_{30}(CO_3)_{12}(NO_3)_6(H_2O)_6]$ chemical formula. This MCA resembles ultrasmall nanoparticles of size with a diameter of approximately 2.2 nm. Within the cluster, lanthanide ions are located in 4 different coordination sites with different local pseudo-symmetries (two distinct D_{3h} sites, one C_s and one C_{4v} site). We proved the solubility and stability of this MCA in acetonitrile and methanol by means of NMR and DLS techniques. The chp ligand triplet state is located up to 24 961 cm^{-1}, enabling an efficient ET for Tb^{3+} ions but not for Eu^{3+} and Sm^{3+}. The quantum yield for **{Tb$_{20}$}** in solid-state was determined as 55.8% due to the efficient sensitization *via* chp ligands. The heterometallic **{Ln$_{20}$}** MCAs represent a milestone in the optical applications of MCAs, as will be discussed in the next section.

Over the last few years, Schipper and Jones groups have developed nanoring-shaped homometallic MCAs with different nuclearities for optically sensing several analytes.[191–195,197–199] Some remarkable examples include **{Yb$_{14}$}**, **{Yb$_{18}$}**, and **{Nd$_{42}$}** for explosives sensing, **{Nd$_{14}$}**, **{Nd$_{18}$}**, and **{Yb$_{18}$}** as antibiotics probes, **{Nd$_{14}$}** for Cu^{2+}, Co^{2+}, H_2PO^{4-}, and F^- detection, **{Eu$_{18}$}** and **{Yb$_{18}$}** for anthrax biomarkers sensing. These MCAs highlight the potential that this class of compound holds in the sensors field. However, as will be discussed in Section 5, we truly believe that studying heterometallic compositions for

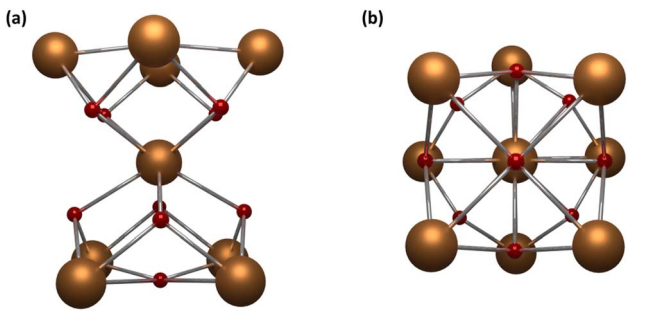

Fig. 4 Metal core structure for **{Ln$_9$}** MCAs. (a) Side view and (b) top view. CCDC number: 956639.[80] Colour code: Dark orange: Ln^{3+}; red: oxygen. Hydrogen atoms were omitted in the structure for clarity.

© 2023 The Author(s). Published by the Royal Society of Chemistry

Open Access Article. Published on 10 2023. Downloaded on 2024/9/11 7:21:17.
This article is licensed under a Creative Commons Attribution-NonCommercial 3.0 Unported Licence.

these nanorings could have more impact in consolidating MCAs as efficient optical materials.

More recently, Bu and co-workers reported the $\{Eu_{48}\}$ and $\{Tb_{48}\}$, the largest luminescent MCA to date.[200] These MCAs feature a nanopillar-like structure constructed from Ln_3 triangles and Ln_5 square pyramid units. The red and green characteristic emissions from Eu^{3+} and Tb^{3+} display a temperature-dependent behaviour over the 88–298 K range, which opens the possibility of using such nanoarchitecture as luminescent thermometers.

As discussed in this section, several examples homometallic luminescent MCAs are reported in the literature. While some unique and innovative systems have been reported, we believe that the true potential of MCAs can only be fully realized through heterometallic structures, which will be discussed in the following section.

5. Optical properties of heterometallic MCAs

Unlike the homometallic systems highlighted above, the use of heterometallic MCAs for optics is in its early stages, with only limited examples reported and discussed in this section. In addition to being intriguing, heterometallic MCAs are more appealing due to the ability to amalgamate different lanthanide ions, regulate ET processes and tuning emission properties for various applications.

The initial illustration of luminescent heterometallic MCA features the well-known nonanuclear hourglass-like MCA with $acac^-$ as the hydrolysis-limiting ligand.[201] By synthesizing MCAs with varying Eu^{3+}/Tb^{3+} ratios, the authors tuned the emission colour output. Despite the authors not fully recognizing its potential, this work marked the beginning of harnessing the power of heterometallic lanthanide-based MCAs for luminescence applications and stands as a milestone achievement in the field.

Inspired by this previous research, we questioned whether we could manipulate lanthanide–lanthanide ET processes within a single MCA unit.

To answer this question, we started our journey into heterometallic MCAs with the hexanuclear wheel, $[Er_3Yb_3(teaH)_6(NO_3)_6]$ (Fig. 5a). As aforementioned, the **{Er_6}** wheel is the first example of a water-soluble MCA showing NIR-to-NIR emissions.[79] In the same work, we demonstrated that by replacing three Er^{3+} atoms with Yb^{3+}, an 85% enhancement of the NIR emission could be attained in the heterometallic **{Er_3Yb_3}** wheel owing to improved absorption of the 980 nm laser by Yb^{3+} ions (Fig. 5b). Furthermore, by changing the solvent to deuterated water, a significant emission increase was achieved, suggesting a strong interaction between the Er^{3+} ions with the OH oscillators from the solvent and pointing out that bulkier ligands would be more efficient in shielding the metal core from the external environment.

Aiming to obtain molecular UC with MCAs, we synthesized a series of pentadecanuclear MCAs containing Yb^{3+} (absorber), Er^{3+} (emitter), and Y^{3+} (optically silent) ions.[92] In these MCAs,

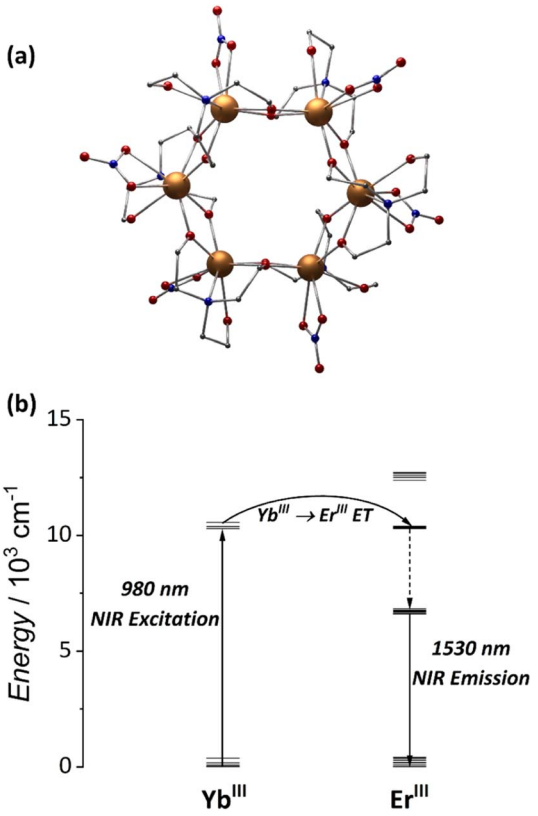

Fig. 5 (a) Single-crystal structure for **{Ln_6}** MCAs (CCDC number: 1958091). (b) Energy-transfer mechanism for the NIR-to-NIR emission.[79] Colour code: Dark orange: Ln^{3+}; grey: carbon; red: oxygen; blue: nitrogen. Hydrogen atoms were omitted in the structure for clarity.

2,2-dimethylolpropionic acid (Hdmp) ligand was used to encapsulate the pentadecanuclear metal core (Fig. 6) in which the lanthanide ions are distributed in three different local symmetries (D_{4d}, D_{2d}, and C_{2v} geometries in a ratio of 1 : 2 : 2). However, similarly to the $teaH^{2-}$ ligand in the **{Er_3Yb_3}** MCA, the use of Hdmp ligand do not effectively prevents interaction with the environment and the molecular UC was only observed at solid-state. Nevertheless, the UC quantum yields (UCQY) obtained in this work were unprecedented for the molecular UC field, reaching values of 10^{-4} to 10^{-3}%. Although low, before this work, the maximum values obtained for UCQY were below 10^{-6}%; hence, this work was pivotal in understanding the superiority of MCAs as molecular upconverters compared with low-nuclearity complexes.

More specifically, in this work, we synthesized five different compositions, **{Er_2Yb_{13}}**, **{$Er_{10}Yb_5$}**, **{$Y_{10}Er_1Yb_4$}**, **{$Y_{13}Er_2$}**, and **{$Y_{10}Er_5$}**. The first composition was synthesized to ensure an excess of donor atoms in relation to acceptors. The second composition aimed the opposite. The third composition added Y^{3+} as an optically inactive atom to distance the optically active atoms. The last two compositions were synthesized containing only Er^{3+} as an optically active ion targeting to evaluate the possibility of Er^{3+}-based ESA UC. These last two compositions do not show any emission upon excitation at 980 and 808 nm,

Open Access Article. Published on 10 2023. Downloaded on 2024/9/11 7:21:17.
This article is licensed under a Creative Commons Attribution-NonCommercial 3.0 Unported Licence.

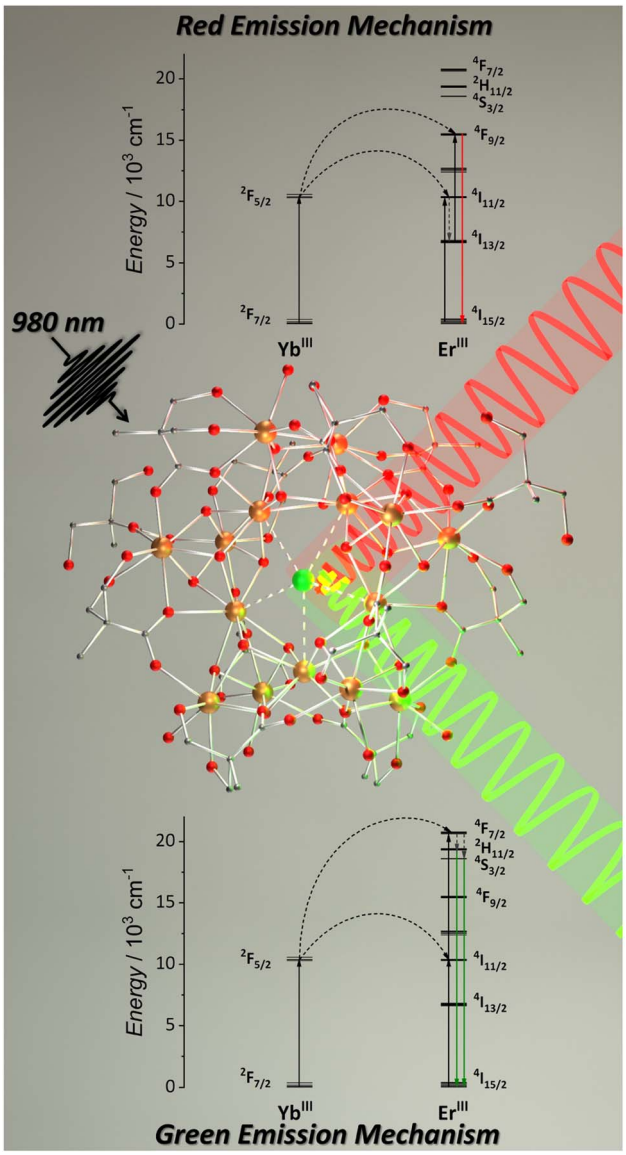

Fig. 6 Single-crystal structure for {Ln_{15}} MCAs (CCDC number: 2023378) and mechanism for red and green UC emissions.[92] Colour code: Dark orange: Ln^{3+}; grey: carbon; red: oxygen. Hydrogen atoms were omitted in the structure for clarity.

confirming the absence of the ESA mechanism. The green and red emission components from Er^{3+} were observed for the other three compositions, occurring *via* the ETU mechanism (Fig. 6). The MCAs show extremely high UCQY compared to other molecular upconverters. The values obtained were 8.3×10^{-3}% for {$Y_{10}Er_1Yb_4$}, 1.5×10^{-3} for {Er_2Yb_{13}}, and 2.8×10^{-4} for {$Er_{10}Yb_5$}. These results indicate that the higher UCQY value observed for {$Y_{10}Er_1Yb_4$} is due to the separation between the optically active ions, reducing the possibility of migration and concentration quenching within the MCA, thus, highlighting the impact of composition control when aiming molecular UC with MCAs.

Simultaneously with the previous work, Charbonnière and co-workers investigated the molecular UC in nonanuclear hourglass-like MCAs.[202] By synthesizing the $[TbYb_8(acac)_{16}(OH)_{10}]$ MCA, they reported the first MCA showing the CUC mechanism with a UCQY of 1×10^{-5}%. More recently,[203] by changing the composition to $[Tb_4Yb_5(acac)_{16}(OH)_{10}]$ and deuterating the ligands, solvent, and the OH^- bridges, the overall performance was significantly improved (UCQY = 2.8×10^{-4}%). In this elegant study, the authors report, for the first time in solution, cooperative upconversion of luminescence with the {Yb_9} MCA. This process results in an emission band at 503 nm when excited by a 980 nm light source.

As previously discussed, our team has made a significant contribution to the field by focusing studying of the {Ln_{20}} class of MCAs (Fig. 7). In our initial investigation with heterometallic {Ln_{20}} MCAs, we successfully isolated a range of Eu^{3+}/Tb^{3+}-based compounds, varying in composition from {Eu_1Tb_{19}} to {Eu_6Tb_{14}}.[81] This allowed us to fine-tune the emission colour output from green to red. This work clearly shows the impact that MCAs can have on the anticounterfeiting materials field, with the development of optical barcodes with the emission colour output finely tuned within the same MCA unit. The success in achieving this resides in how the composition control impacts the Tb^{3+} to Eu^{3+} ET processes. The ET efficiency is more than double in {Eu_6Tb_{14}} than observed for {Eu_2Tb_{18}} due to the increased number of acceptors within the same MCA unit. We have also been able to observe Tb^{3+} to Sm^{3+} ET by exploring {Sm_4Tb_{16}}, {$Sm_{10}Tb_{10}$}, and {$Sm_{16}Tb_4$} compositions, each one containing different ratios between Sm^{3+} and Tb^{3+} emission components. Additionally, by finely controlling the ratio of Eu^3, Gd^{3+}, and Tb^{3+} atoms and precisely selecting a suitable excitation energy (355 nm) we have been able to obtain white-light emission with the {$Eu_3Gd_5Tb_{12}$} composition due to a favoured blue emission component from the chp ligand when adding Gd^{3+} to the MCA.

We further explored the Tb^{3+} to Eu^{3+} ET in {Ln_{20}} MCAs for luminescence thermometry applications.[93] We synthesized {Ln_{20}} MCAs with four different compositions in which we kept the Eu^{3+}/Tb^{3+} ratios constant (4 : 1). The {Eu_4Tb_{16}}, {$Eu_3Gd_5Tb_{12}$}, {$Eu_2Gd_{10}Tb_8$}, and {$Eu_1Gd_{15}Tb_4$} compositions were synthesized, and the temperature-dependent emission properties were evaluated in an acetonitrile solution (0.1 mg mL^{-1}). The increasing amount of Gd^{3+} atoms aimed for a physical distancing between the donor (Tb^{3+}) and acceptor (Eu^{3+}) atoms while keeping the ratios constant. Our results indicated a decrease in the Tb^3 to Eu^{3+} ET efficiency from 86.7% for {Eu_4Tb_{16}} to 60.5% for {$Eu_1Gd_{15}Tb_4$} MCA. This reduction of the ET efficiency negatively impacted the thermometric performance. For {Eu_4Tb_{16}}, a maximum relative sensitivity of 4.17% °C^{-1} was obtained, decreasing to 1.82% °C^{-1} for {$Eu_1Gd_{15}Tb_4$}.

In this work, we also compared the photophysical and thermometric performances of {Eu_4Tb_{16}} in solution and solid-state, which shows no difference, suggesting a high composition homogeneity and proving that the ET processes operate solely within the MCA unit. The relative sensitivity obtained for these {Ln_{20}} MCAs are in the same range as other Ln^{3+}-based molecular luminescent ratiometric thermometers;[204–219] however, the fact that the ET process occurs within the same

© 2023 The Author(s). Published by the Royal Society of Chemistry

Open Access Article. Published on 10 2023. Downloaded on 2024/9/11 7:21:17.
This article is licensed under a Creative Commons Attribution-NonCommercial 3.0 Unported Licence.

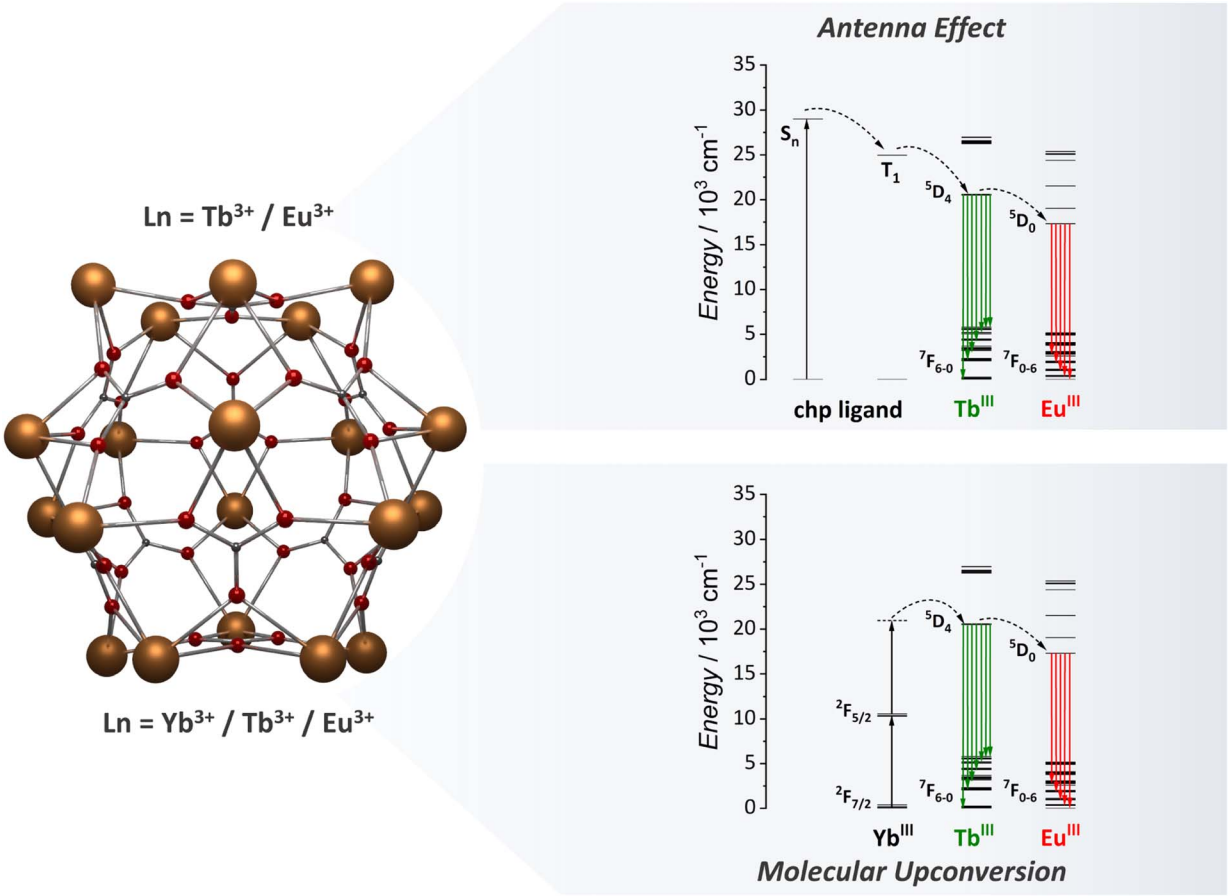

Fig. 7 Metal core structure of the {Ln_{20}} MCAs (CCDC number: 2023766)[81] and the energy transfer mechanism for antenna effect and UC emissions.[81,95] Colour code: Dark orange: Ln^{3+}; grey: carbon; red: oxygen. Hydrogen atoms were omitted in the structure for clarity.

cluster unit is a great advantage, as it allows us to control the performance at an individual cluster level.

More recently, our group used this same system to explore a new luminescence thermometry approach, the time-gated luminescence thermometry.[96] We take advantage of the Tb^{3+} to Eu^{3+} ET processes and different decay dynamics for {$\mathbf{Eu_5Tb_{15}}$} MCA to implement a strategy in which a pulsed lamp is used to excite the sample and various delays were employed on the detection channel. This promising new approach that can help move from laboratory equipment to real-life applications by eliminating any background emission that can plague the luminescence thermometry implementation. This approach also resulted in a 250% enhancement of the relative thermal sensitivity for {$\mathbf{Eu_5Tb_{15}}$} MCA, from 2.79 to 9.78% $°C^{-1}$.

After exploring the ligand-based sensitization for {$\mathbf{Ln_{20}}$} MCAs and understanding the composition control impact for optical barcoding[81] and luminescence thermometry,[93] we moved one step further, targeting the use of {$\mathbf{Ln_{20}}$} as molecular upconverters.[95] To tap into this mechanism, we synthesized {$\mathbf{Gd_{11}Tb_2Yb_7}$}, aiming for a cooperative UC mechanism (Fig. 7). For this system, Yb^{3+} acts as the absorber (donor) species, Tb^{3+} as the emitter ion, and Gd^{3+} as an optically silent ion to guarantee a distancing of Tb^{3+} ions within the structure. Upconverted emission was successfully observed upon a 980 nm laser excitation. The rigid spherical shape of the {$\mathbf{Ln_{20}}$} MCA, which resembles spherical nanoparticles, enabled the reduction of molecular vibrations, minimizing possible vibrational mediated quenching pathways, thus resulting in a UCQY of 1.04×10^{-4}%. Intending further to expand the possibilities in the molecular UC field, we target the demonstration of luminescence thermometry obtained *via* the molecular UC demonstrated in this work. It should be noted that prior to this work, molecular UC works were limited to demonstrating the presence of the mechanism, and there was no previous report of potential applications. To tap into the luminescence thermometry demonstration, we replaced some of the Gd^{3+} ions with Eu^{3+} intending to access the $Yb^{3+} \rightarrow Tb^{3+} \rightarrow Eu^{3+}$ ET process (Fig. 7). Four different compositions were synthesized, namely, {$\mathbf{Eu_8Gd_3Tb_2Yb_7}$}, {$\mathbf{Eu_9Gd_2Tb_2Yb_7}$}, {$\mathbf{Eu_{10}Gd_1Tb_2Yb_7}$}, and {$\mathbf{Eu_{11}Tb_2Yb_7}$}, and the temperature dependent UC was measured. We have observed considerable changes in the ratios of Tb^{3+} and Eu^{3+} emission bands and thermometric performances, reaching a maximum relative sensitivity of 3.05% $°C^{-1}$ for {$\mathbf{Eu_9Gd_2Tb_2Yb_7}$} MCA. The success in implementing molecular UC-based luminescence thermometry with {$\mathbf{Ln_{20}}$} opens new avenues for molecular upconverters.

After observing Yb^{3+}/Tb^{3+}-based cooperative UC with some of the {$\mathbf{Ln_{20}}$} MCAs, we decide to explore the Yb^{3+}/Ho^{3+} pair

Open Access Article. Published on 10 2023. Downloaded on 2024/9/11 7:21:17.
This article is licensed under a Creative Commons Attribution-NonCommercial 3.0 Unported Licence.

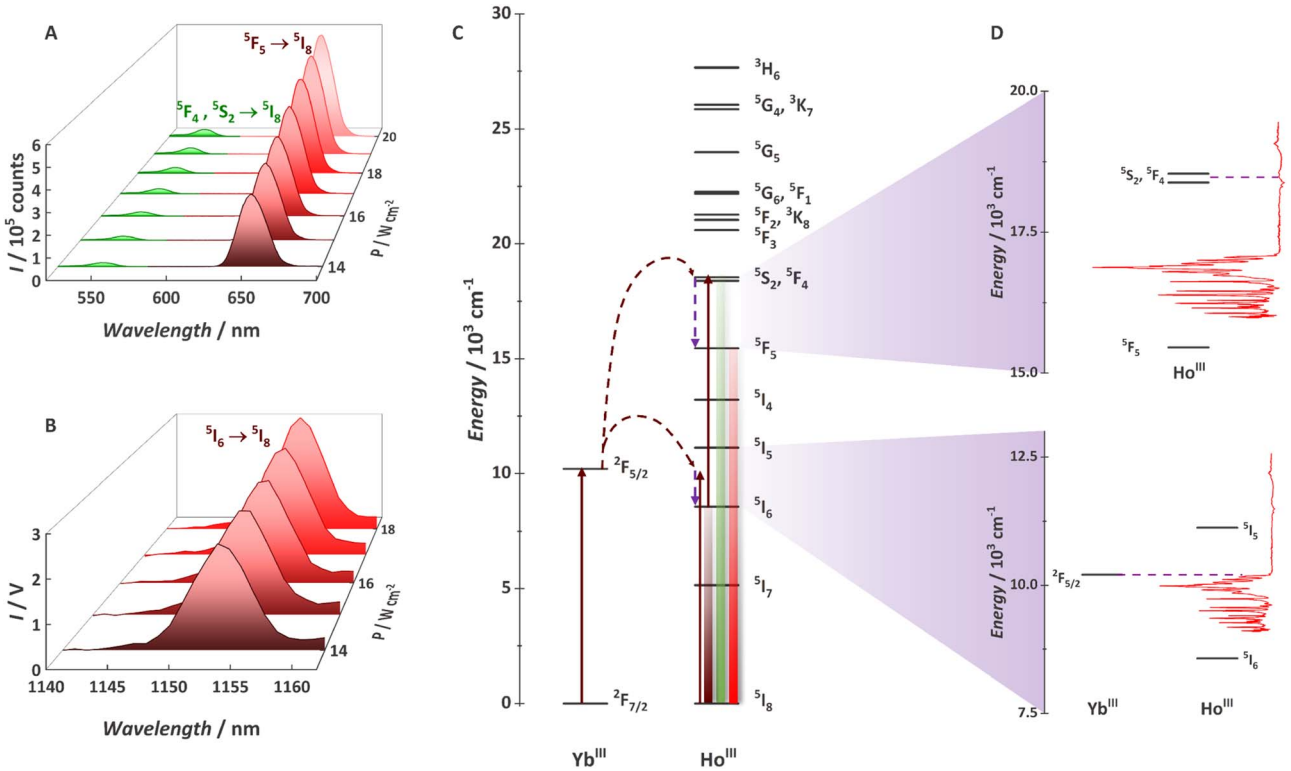

Fig. 8 (A) Upconversion spectra for a 0.1 mg mL^{-1} deuterated methanol solution of **{Gd$_8$Ho$_2$Yb$_{10}$}** obtained at 20 °C with the incident laser power (λ_{exc} = 980 nm/ν_{ex} = 10 204 cm^{-1}) focused on a spot size of ~0.03 cm^2. (B) NIR-to-NIR spectra of **{Gd$_8$Ho$_2$Yb$_{10}$}**. (C) Partial energy level diagram for the MCA showing Yb^{III} and Ho^{III} levels. (D) Coupling between the vibration and electronic levels. Adapted from ref. 94 with permission from the Royal Society of Chemistry.

(Fig. 8).[94] Although widely demonstrated for nanoparticles, glasses, and other classes of low-phonon materials,[220–224] Ho^{3+} UC was never observed with a molecular system. The main reason is the mismatching between Yb^{3+} (donor) and Ho^{3+} (acceptor) electronic states. In this work, we have shown for the first-time molecular UC (Fig. 8a) and molecular NIR-to-NIR emission (Fig. 8b) based on the Yb^{3+}/Ho^{3+} pair. The UC process occurs *via* the ETU mechanism with the absorption of two 980 nm photons, thus populating Ho^{3+} green emitter states ($^5S_2$ and $^5F_4$). Photons can be emitted by this state or non-radiatively decay to the red emitter state ($^5F_5$). Additionally, we proved that molecular vibrations are not always the villains for molecular UC with the νC=O and/or νC=C$_{aromatic}$ at ~1595 cm^{-1} helping to bridge the gap between donor and acceptor levels (Fig. 8c and d) and allowing the energy-transfer UC mechanism. For the **{Gd$_8$Ho$_2$Yb$_{10}$}** MCA, a UCQY of 5.24 × 10^{-6}% was observed, thus expanding the molecular UC possibilities by adding another emitter ion as a potential candidate.

These previous works highlight the versatility of heterometallic MCAs as highly efficient optical materials. The **{Ln$_{20}$}** MCA has been demonstrated as an impressive toolbox for both ligand-sensitized and UC luminescence, with a significant impact in applications which require fine control of ET processes such as luminescent thermometry and anti-counterfeiting materials.

6. Conclusions and outlook

In this perspective, we highlighted recent advances in using high-nuclearity lanthanide-based MCAs as efficient optical materials. Our research group has shown that these materials have the potential to be the next generation of highly emissive compounds with unprecedented composition control and fine tuning of energy transfer (ET) process. This precise control of ET has significant implications in attaining high-performance luminescent materials, expanding the possibilities of applications in which colour output and/or ET processes play pivotal roles as luminescent thermometers and optical barcodes for anti-counterfeiting applications.

As discussed in Section 4 and summarized in Table 1, there are a small, but much higher number of examples related to homometallic luminescent MCAs. Further exploration and consolidation of this class of compounds could be achieved by evaluating these systems with mixed metal strategy. We believe that some of these underexplored homometallic systems, could result in excellent materials for luminescence thermometry, optical barcodes, and molecular upconverters upon investigation of their heterometallic counter parts.

In the field of molecular UC, MCAs already represent a turning point. The rigid metal core structure and the multiple metal ions enabled four orders of magnitude enhancement for UCQY when compared with low-nuclearity molecular

© 2023 The Author(s). Published by the Royal Society of Chemistry

Open Access Article. Published on 10 2023. Downloaded on 2024/9/11 7:21:17.
This article is licensed under a Creative Commons Attribution-NonCommercial 3.0 Unported Licence.

upconverters, approaching the UCQY values observed for ultrasmall nanoparticles.

As in the case of all emerging fields, much more can and needs to be done to its consolidation. Up to now, the highest nuclearity explored for heterometallic luminescent MCAs is twenty. Efforts should be focused on understanding whether higher nuclearities can be beneficial or detrimental to the ET processes within the metal core. From one side, one can expect that more metal in the core will allow greater control of the ET and colour outputs, being valuable for thermometry and anti-counterfeiting applications. However, the great majority of highest-nuclearity MCAs (60 and higher metal ions) show a hollow structure with a void space on the centre of the cluster; thus, it is also possible that increasing the nuclearities in hollow MCAs can result in a detrimental distancing of the optically active ions, resulting in a poorer ET efficiency. Therefore, systematic studies with higher nuclearity heterometallic MCAs will dictate the future directions of the field in the coming years.

Data availability

As a perspective article, no new experimental or computational data are included.

Author contributions

All authors equally contributed to the manuscript preparation and writing.

Conflicts of interest

There are no conflicts to declare.

Acknowledgements

We thank the University of Ottawa, the CFI, and the NSERC for financial support of this work.

References

1 J.-C. G. Bünzli and S. V. Eliseeva, *Chem. Sci.*, 2013, **4**, 1939.
2 A. de Bettencourt-Dias, *Dalton Trans.*, 2007, **2007**, 2229.
3 X. Qin, X. Liu, W. Huang, M. Bettinelli and X. Liu, *Chem. Rev.*, 2017, **117**, 4488.
4 Z. Xia and Q. Liu, *Prog. Mater. Sci.*, 2016, **84**, 59.
5 S. V. Eliseeva and J.-C. G. Bünzli, *Chem. Soc. Rev.*, 2010, **39**, 189.
6 J.-C. G. Bünzli, *Trends Chem.*, 2019, **1**, 751.
7 X. Dong Wang, O. S. Wolfbeis and R. J. Meier, *Chem. Soc. Rev.*, 2013, **42**, 7834.
8 L. H. Fischer, G. S. Harms and O. S. Wolfbeis, *Angew. Chem., Int. Ed.*, 2011, **50**, 4546.
9 M. L. Cable, J. P. Kirby, H. B. Gray and A. Ponce, *Acc. Chem. Res.*, 2013, **46**, 2576.
10 C. D. S. Brites, P. P. Lima, N. J. O. Silva, A. Millán, V. S. Amaral, F. Palacio and L. D. Carlos, *Nanoscale*, 2012, **4**, 4799.
11 C. D. S. Brites, S. Balabhadra and L. D. Carlos, *Adv. Opt. Mater.*, 2019, **7**, 1801239.
12 A. Ćirić, S. Stojadinović and M. D. Dramićanin, *J. Lumin.*, 2019, **216**, 116749.
13 C. D. S. Brites, P. P. Lima, N. J. O. Silva, A. Millan, V. S. Amaral, F. Palacio and L. D. Carlos, *New J. Chem.*, 2011, **35**, 1177.
14 P. Netzsch, M. Hämmer, E. Turgunbajew, T. P. van Swieten, A. Meijerink, H. A. Höppe and M. Suta, *Adv. Opt. Mater.*, 2022, **10**, 2200059.
15 A. A. Ansari, A. K. Parchur, M. K. Nazeeruddin and M. M. Tavakoli, *Coord. Chem. Rev.*, 2021, **444**, 214040.
16 J. Rocha, C. D. S. Brites and L. D. Carlos, *Chem.–Eur. J.*, 2016, **22**, 14782.
17 G. Brunet, R. Marin, M.-J. Monk, U. Resch-Genger, D. A. Gálico, F. A. Sigoli, E. A. Suturina, E. Hemmer and M. Murugesu, *Chem. Sci.*, 2019, **10**, 6799.
18 D. A. Gálico, R. Marin, G. Brunet, D. Errulat, E. Hemmer, F. A. Sigoli, J. O. Moilanen and M. Murugesu, *Chem.–Eur. J.*, 2019, **25**, 14625.
19 R. M. Diaz-Rodriguez, D. A. Gálico, D. Chartrand, E. A. Suturina and M. Murugesu, *J. Am. Chem. Soc.*, 2022, **144**, 912.
20 F. M. Cabral, D. A. Gálico, I. O. Mazali and F. A. Sigoli, *Inorg. Chem. Commun.*, 2018, **98**, 29.
21 D. Parker, *Coord. Chem. Rev.*, 2000, **205**, 109.
22 C. M. G. dos Santos, A. J. Harte, S. J. Quinn and T. Gunnlaugsson, *Coord. Chem. Rev.*, 2008, **252**, 2521.
23 S. Shinoda and H. Tsukube, *Analyst*, 2011, **136**, 431.
24 B. V. Harbuzaru, A. Corma, F. Rey, J. L. Jordá, D. Ananias, L. D. Carlos and J. Rocha, *Angew. Chem., Int. Ed.*, 2009, **48**, 6476.
25 A. M. Kaczmarek, Y. -Y. Liu, C. Wang, B. Laforce, L. Vincze, P. Van Der Voort, K. Van Hecke and R. Van Deun, *Adv. Funct. Mater.*, 2017, **27**, 1700258.
26 E. J. New, D. Parker, D. G. Smith and J. W. Walton, *Curr. Opin. Chem. Biol.*, 2010, **14**, 238.
27 Y. Zhao and D. Li, *J. Mater. Chem. C*, 2020, **8**, 12739.
28 X. Wang, H. Chang, J. Xie, B. Zhao, B. Liu, S. Xu, W. Pei, N. Ren, L. Huang and W. Huang, *Coord. Chem. Rev.*, 2014, **273**, 201.
29 L.-N. Sun, H. Peng, M. I. J. Stich, D. Achatz and O. S. Wolfbeis, *Chem. Commun.*, 2009, **33**, 5000.
30 M. G. Lahoud, R. C. G. Frem, D. A. Gálico, G. Bannach, M. M. Nolasco, R. A. S. Ferreira and L. D. Carlos, *J. Lumin.*, 2016, **170**, 357.
31 L. Li, Q. Chen, Z. Niu, X. Zhou, T. Yang and W. Huang, *J. Mater. Chem. C*, 2016, **4**, 1900.
32 H. Wang, X. Wang, M. Liang, G. Chen, R.-M. Kong, L. Xia and F. Qu, *Anal. Chem.*, 2020, **92**, 3366.
33 M. Runowski, P. Woźny and I. R. Martín, *J. Mater. Chem. C*, 2021, **9**, 4643.
34 M. Runowski, P. Woźny, N. Stopikowska, Q. Guo and S. Lis, *ACS Appl. Mater. Interfaces*, 2019, **11**, 4131.
35 M. Runowski, P. Woźny, N. Stopikowska, I. R. Martín, V. Lavín and S. Lis, *ACS Appl. Mater. Interfaces*, 2020, **12**, 43933.

Open Access Article. Published on 10 2023. Downloaded on 2024/9/11 7:21:17.
This article is licensed under a Creative Commons Attribution-NonCommercial 3.0 Unported Licence.

36 K. Du, J. Feng, X. Gao and H. Zhang, *Light Sci. Appl.*, 2022, **11**, 222.
37 W. Yang, X. Li, D. Chi, H. Zhang and X. Liu, *Nanotechnol*, 2014, **25**, 482001.
38 F. Wang, D. Banerjee, Y. Liu, X. Chen and X. Liu, *Analyst*, 2010, **135**, 1839.
39 S. Han, R. Deng, X. Xie and X. Liu, *Angew. Chem., Int. Ed.*, 2014, **53**, 11702.
40 F. Wang, Y. Han, C. S. Lim, Y. Lu, J. Wang, J. Xu, H. Chen, C. Zhang, M. i. Hong and X. Liu, *Nature*, 2010, **463**, 1061.
41 J.-C. G. Bünzli, *Coord. Chem. Rev.*, 2015, **293**, 19.
42 C. Wei, L. Ma, H. B. Wei, Z. W. Liu, Z. Q. Bian and C. H. Huang, *Sci. China: Technol. Sci.*, 2018, **61**, 1265.
43 S. Faulkner, S. J. A. Pope and B. P. Burton-Pye, *Appl. Spectrosc. Rev.*, 2005, **40**, 1.
44 C. Andraud and O. Maury, *Eur. J. Inorg. Chem.*, 2009, **2009**, 4357.
45 L. Armelao, S. Quici, F. Barigelletti, G. Accorsi, G. Bottaro, M. Cavazzini and E. Tondello, *Coord. Chem. Rev.*, 2010, **254**, 487.
46 X.-Y. Zheng, J. Xie, X.-J. Kong, L.-S. Long and L.-S. Zheng, *Coord. Chem. Rev.*, 2019, **378**, 222.
47 A. T. Wagner and P. W. Roesky, *Eur. J. Inorg. Chem.*, 2016, **2016**, 782.
48 Z. Zhang, Y. Zhang and Z. Zheng, *Struct. Bonding*, 2017, **173**, 1.
49 A. V. Virovets, E. Peresypkina and M. Scheer, *Chem. Rev.*, 2021, **121**, 14485.
50 X.-M. Luo, Y.-K. Li, X.-Y. Dong and S.-Q. Zang, *Chem. Soc. Rev.*, 2023, **52**, 383.
51 J.-C. G. Bünzli and S. V. Eliseeva, in *Lanthanide Luminescence*, ed. P. Hänninen and H. Härmä, Springer Berlin Heidelberg, Berlin, Heidelberg, 2010, vol. 7, pp. 1–45.
52 C. Görller-Walrand and K. Binnemans, in *Handbook on the Physics and Chemistry of Rare Earths*, ed. K. A. Gschneidner Jr and L. R. Eyring, Elsevier Science B. V., 1998, vol. 25, pp. 101–264.
53 C. Görller-Walrand and K. Binnemans, in *Handbook on the Physics and Chemistry of Rare Earths*, ed. K. A. Gschneidner Jr and L. Eyring, Elsevier Science B. V., 1996, vol. 23, pp. 121–283.
54 K. Binnemans, *Coord. Chem. Rev.*, 2015, **295**, 1.
55 J.-C. G. Bünzli and C. Piguet, *Chem. Soc. Rev.*, 2005, **34**, 1048.
56 L. Qin, G.-J. Zhou, Y.-Z. Yu, H. Nojiri, C. Schröder, R. E. P. Winpenny and Y.-Z. Zheng, *J. Am. Chem. Soc.*, 2017, **139**, 16405.
57 R. Sen, D. K. Hazra, M. Mukherjee and S. Koner, *Eur. J. Inorg. Chem.*, 2011, **2011**, 2826.
58 Y.-L. Li, H.-L. Wang, Z.-H. Zhu, F.-P. Liang and H.-H. Zou, *Inorg. Chem.*, 2022, **61**, 10101.
59 M. Wu, F. Jiang, D. Yuan, J. Pang, J. Qian, S. A. AL-Thabaitic and M. Hong, *Chem. Commun.*, 2014, **50**, 1113.
60 L. Qin, Y.-Z. Yu, P.-Q. Liao, W. Xue, Z. Zheng, X.-M. Chen and Y.-Z. Zheng, *Adv. Mater.*, 2016, **28**, 10772.
61 X.-Y. Li, H.-F. Su, Q.-W. Li, R. Feng, H.-Y. Bai, H.-Y. Chen, J. Xu and X.-H. Bu, *Angew. Chem., Int. Ed.*, 2019, **58**, 10184.
62 X.-Y. Zheng, X.-J. Kong, Z. Zheng, L.-S. Long and L.-S. Zheng, *Acc. Chem. Res.*, 2018, **51**, 517.
63 Z.-M. Zhang, K. H. Zangana, A. K. Kostopoulos, M.-L. Tong and R. E. P. Winpenny, *Dalton Trans.*, 2016, **45**, 9041.
64 F.-S. Guo, Y.-C. Chen, L.-L. Mao, W.-Q. Lin, J.-D. Leng, R. Tarasenko, M. Orendáč, J. Prokleška, V. Sechovský and M.-L. Tong, *Chem.–Eur. J.*, 2013, **19**, 14876.
65 X.-Y. Zheng, J.-B. Peng, X.-J. Kong, L.-S. Long and L.-S. Zheng, *Inorg. Chem. Front.*, 2016, **3**, 320.
66 J.-B. Peng, Q.-C. Zhang, X.-J. Kong, Y.-P. Ren, L.-S. Long, R.-B. Huang, L.-S. Zheng and Z. Zheng, *Angew. Chem., Int. Ed.*, 2011, **50**, 10649.
67 W. Huang, Z. Zhang, Y. Wu, W. Chen, D. A. Rotsch, L. Messerle and Z. Zheng, *Inorg. Chem. Front.*, 2021, **8**, 26.
68 T.-Q. Song, J. Dong, A.-F. Yang, X.-J. Che, H.-L. Gao, J.-Z. Cui and B. Zhao, *Inorg. Chem.*, 2018, **57**, 3144.
69 Y.-L. Li, H.-L. Wang, Z.-H. Zhu, J. Li, H.-H. Zou and F.-P. Liang, *Inorg. Chem.*, 2021, **60**, 16794.
70 P. Hu, S. Li, L. Cao, A. Liu, G.-L. Zhuang, L. Ji and B. Li, *ACS Omega*, 2022, **7**, 38782.
71 Z. Li, D. Wang, Z. Zhou, G. Zhao, Q. Li, Y. Bi and Z. Zheng, *Inorg. Chem.*, 2022, **61**, 20814.
72 T.-Q. Lu, H. Xu, L.-T. Cheng, X.-T. Wang, C. Chen, L. Cao, G.-L. Zhuang, J. Zheng and X.-Y. Zheng, *Inorg. Chem.*, 2022, **61**, 8861.
73 Z.-R. Luo, H.-L. Wang, Z.-H. Zhu, T. Liu, X.-F. Ma, H.-F. Wang, H.-H. Zou and F.-P. Liang, *Commun. Chem.*, 2020, **3**, 30.
74 J. R. McBride, A. D. Dukes III, M. A. Schreuder and S. J. Rosenthal, *Chem. Phys. Lett.*, 2010, **498**, 1.
75 B. H. Kim, M. J. Hackett, J. Park and T. Hyeon, *Chem. Mater.*, 2014, **26**, 59.
76 K. Zarschler, L. Rocks, N. Licciardello, L. Boselli, E. Polo, K. P. Garcia, L. De Cola, H. Stephan and K. A. Dawson, *Nanomedicine*, 2016, **12**, 1663.
77 I. Halimi, E. M. Rodrigues, S. L. Maurizio, H.-Q. T. Sun, M. Grewal, E. M. Boase, N. Liu, R. Marin and E. Hemmer, *J. Mater. Chem. C*, 2019, **7**, 15364.
78 N. Liu, N. Gobeil, P. Evers, I. Gessner, E. M. Rodrigues and E. Hemmer, *Dalton Trans.*, 2020, **49**, 16204.
79 D. A. Gálico, J. S. Ovens and M. Murugesu, *Nanoscale*, 2020, **12**, 11435.
80 T. Nakanishi, Y. Suzuki, Y. Doi, T. Seki, H. Koizumi, K. Fushimi, K. Fujita, Y. Hinatsu, H. Ito, K. Tanaka and Y. Hasegawa, *Inorg. Chem.*, 2014, **53**, 7635.
81 D. A. Gálico, A. A. Kitos, J. S. Ovens, F. A. Sigoli and M. Murugesu, *Angew. Chem., Int. Ed.*, 2021, **60**, 6130.
82 W. Huang, W. Chen, Q. Bai, Z. Zhang, M. Feng and Z. Zheng, *Angew. Chem., Int. Ed.*, 2022, **134**, e202205385.
83 X.-Y. Zheng, Y.-H. Jiang, G.-L. Zhuang, D.-P. Liu, H.-G. Liao, X.-J. Kong, L.-S. Long and L.-S. Zheng, *J. Am. Chem. Soc.*, 2017, **139**, 18178.
84 R. Wang, Z. Zheng, T. Jin and R. J. Staples, *Angew. Chem., Int. Ed.*, 1999, **38**, 1813.
85 R. Wang, H. D. Selby, H. Liu, M. D. Carducci, T. Jin, Z. Zheng, J. W. Anthis and R. J. Staples, *Inorg. Chem.*, 2002, **41**, 278.

© 2023 The Author(s). Published by the Royal Society of Chemistry

Open Access Article. Published on 10 2023. Downloaded on 2024/9/11 7:21:17.
This article is licensed under a Creative Commons Attribution-NonCommercial 3.0 Unported Licence.

86 Z. Zheng and R. Wang, *Comments Inorg. Chem.*, 2000, **22**, 1.
87 J. Dong, P. Cui, P.-F. Shi, P. Cheng and B. Zhao, *J. Am. Chem. Soc.*, 2015, **137**, 15988.
88 X.-M. Luo, Z.-B. Hu, Q.-F. Lin, W. Cheng, J.-P. Cao, C.-H. Cui, H. Mei, Y. Song and Y. Xu, *J. Am. Chem. Soc.*, 2018, **140**, 11219.
89 X.-M. Luo, N.-F. Li, Q.-F. Lin, J.-P. Cao, P. Yuan and Y. Xu, *Inorg. Chem. Front.*, 2020, **7**, 2072.
90 X.-J. Kong, Y. Wu, L.-S. Long, L.-S. Zheng and Z. Zheng, *J. Am. Chem. Soc.*, 2009, **131**, 6918.
91 J.-B. Peng, X.-J. Kong, Q.-C. Zhang, M. Orendac, J. Prokleska, Y. P. Ren, L.-S. Long, Z. Zheng and L.-S. Zheng, *J. Am. Chem. Soc.*, 2014, **136**, 17938.
92 D. A. Gálico, J. S. Ovens, F. A. Sigoli and M. Murugesu, *ACS Nano*, 2021, **15**, 5580.
93 D. A. Gálico and M. Murugesu, *ACS Appl. Mater. Interfaces*, 2021, **13**, 47052.
94 D. A. Gálico, R. Ramdani and M. Murugesu, *Nanoscale*, 2022, **14**, 9675.
95 D. A. Gálico and M. Murugesu, *Angew. Chem., Int. Ed.*, 2022, **61**, e202204839.
96 D. A. Gálico and M. Murugesu, *Nanoscale*, 2023, **15**, 5778.
97 O. Laporte and W. F. Meggers, *J. Opt. Soc. Am.*, 1925, **11**, 459.
98 D. Errulat, R. Marin, D. A. Gálico, K. L. M. Harriman, A. Pialat, B. Gabidullin, F. Iikawa, O. D. D. Couto Jr, J. O. Moilanen, E. Hemmer, F. A. Sigoli and M. Murugesu, *ACS Cent. Sci.*, 2019, **5**, 1187.
99 W. T. Carnall, P. R. Fields and K. Rajnak, *Argonne National Laboratory – Technical Report*, 1968.
100 F. Wang, R. Deng, J. Wang, Q. Wang, Y. Han, H. Zhu, X. Chen and X. Liu, *Nat. Mater.*, 2011, **10**, 968.
101 F. Wang and X. Liu, *J. Am. Chem. Soc.*, 2008, **130**, 5642.
102 X. Qin, J. Xu, Y. Wu and X. Liu, *ACS Cent. Sci.*, 2019, **5**, 29.
103 S. Wen, J. Zhou, K. Zheng, A. Bednarkiewicz, X. Liu and D. Jin, *Nat. Commun.*, 2018, **9**, 2415.
104 Z. Lei, X. Ling, Q. Mei, S. Fu, J. Zhang and Y. Zhang, *Adv. Mater.*, 2020, **32**, 1906225.
105 Y. Zhong, I. Rostami, Z. Wang, H. Dai and Z. Hu, *Adv. Mater.*, 2015, **27**, 6418.
106 G. Bao, K.-L. Wong, D. Jin and P. A. Tanner, *Light Sci. Appl.*, 2018, **7**, 96.
107 Y. Kitagawa, K. Matsuda, P. P. F. da Rosa, K. Fushimi and Y. Hasegawa, *Chem. Commun.*, 2021, **57**, 8047.
108 S. Faulkner and S. J. A. Pope, *J. Am. Chem. Soc.*, 2003, **125**, 10526.
109 F. Auzel, *Chem. Rev.*, 2004, **104**, 139.
110 S. Liu, L. Yan, J. Huang, Q. Zhang and B. Zhou, *Chem. Soc. Rev.*, 2022, **51**, 1729.
111 H. Dong, L.-D. Sun and C.-H. Yan, *Nanoscale*, 2013, **5**, 5703.
112 B. Zhou, B. Shi, D. Jin and X. Liu, *Nat. Nanotechnol.*, 2015, **10**, 924.
113 S. I. Weissman, *J. Chem. Phys.*, 1942, **10**, 214.
114 G. A. Crosby, R. E. Whan and R. M. Alire, *J. Chem. Phys.*, 1961, **34**, 743.
115 G. A. Crosby, R. E. Whan and J. J. Freeman, *J. Phys. Chem.*, 1962, **66**, 2493.
116 F. J. Steemers, W. Verboom, D. N. Reinhoudt, E. B. van der Tol and J. W. Verhoeven, *J. Am. Chem. Soc.*, 1995, **117**, 9408.
117 M. J. Beltrán-Leiva, E. Solis-Céspedes and D. Páez-Hernández, *Dalton Trans.*, 2020, **49**, 7444.
118 D. A. Gálico, E. R. Souza, I. O. Mazali and F. A. Sigoli, *J. Lumin.*, 2019, **210**, 397.
119 M. Latva, H. Takalo, V.-M. Mukkala, C. Matachescu, J. C. Rodríguez-Ubis and J. Kankare, *J. Lumin.*, 1997, **75**, 149.
120 N. Bloembergen, *Phys. Rev. Lett.*, 1959, **2**, 84.
121 F. Auzel, *C. R. Acad. Sci.*, 1966, **263**, 819.
122 V. V. Ovsyakin and P. P. Feoflov, *JETP Lett.*, 1966, **4**, 317.
123 R. Rafique, S. K. Kailasa and T. J. Park, *Trends Anal. Chem.*, 2019, **120**, 115646.
124 M. Zhao, B. Li, P. Wang, L. Lu, Z. Zhang, L. Liu, S. Wang, D. Li, R. Wang and F. Zhang, *Adv. Mater.*, 2018, **30**, 1804982.
125 Q. Liu, W. Feng and F. Li, *Coord. Chem. Rev.*, 2014, **273**, 100.
126 Y.-F. Wang, G.-Y. Liu, L.-D. Sun, J.-W. Xiao, J.-C. Zhou and C.-H. Yan, *ACS Nano*, 2013, **7**, 7200.
127 M. V. Da Costa, S. Doughan, Y. Han and U. J. Krull, *Anal. Chim. Acta*, 2014, **832**, 1.
128 S. Xu, S. Huang, Q. He and L. Wang, *Trends Anal. Chem.*, 2015, **66**, 72.
129 Y. Xie, Y. Sun, J. Sun, Y. Wang, S. Yu, B. Zhou, B. Xue, X. Zheng, H. Liu and B. Dong, *Inorg. Chem. Front.*, 2023, **10**, 93.
130 N. M. Idris, M. K. Gnanasammandhan, J. Zhang, P. C. Ho, R. Mahendran and Y. Zhang, *Nat. Med.*, 2012, **18**, 1580.
131 M. R. Hamblin, *Dalton Trans.*, 2018, **47**, 8571.
132 Y. Liu, X. Meng and W. Bu, *Coord. Chem. Rev.*, 2019, **379**, 82.
133 Y. Liu, Y. Liu, W. Bu, C. Cheng, C. Zuo, Q. Xiao, Y. Sun, D. Ni, C. Zhang, J. Liu and J. Shi, *Angew. Chem., Int. Ed.*, 2015, **54**, 8105.
134 B. Zheng, H. Wang, H. Pan, C. Liang, W. Ji, L. Zhao, H. Chen, X. Gong, X. Wu and J. Chang, *ACS Nano*, 2017, **11**, 11898.
135 S. Chen, A. Z. Weitemier, X. Zeng, L. He, X. Wang, Y. Tao, A. J. Y. Huang, Y. Hashimotodani, M. Kano, H. Iwasaki, L. K. Parajuli, S. Okabe, D. B. L. Teh, A. H. All, I. Tsutsui-Kimura, K. F. Tanaka, X. Liu and T. J. McHugh, *Science*, 2018, **359**, 679.
136 A. H. All, X. Zeng, D. B. L. Teh, Z. Yi, A. Prasad, T. Ishizuka, N. Thakor, Y. Hiromu and X. Liu, *Adv. Mater.*, 2019, **31**, 180347.
137 Z. Wang, M. Hu, X. Ai, Z. Zhang and B. Xing, *Adv. Biosyst.*, 2019, **3**, 1800233.
138 X. Wu, Y. Zhang, K. Takle, O. Bilsel, Z. Li, H. Lee, Z. Zhang, D. Li, W. Fan, C. Duan, E. M. Chan, C. Lois, Y. Xiang and G. Han, *ACS Nano*, 2016, **10**, 1060.
139 T. Hebert, R. Wannemacher, W. Lenth and R. M. Macfarlane, *Appl. Phys. Lett.*, 1990, **57**, 1727.
140 H. Zhu, X. Chen, L. M. Jin, Q. J. Wang, F. Wang and S. F. Yu, *ACS Nano*, 2013, **7**, 11420.
141 T. Wang, H. Yu, C. K. Siu, J. B. Qiu, X. H. Xu and S. F. Yu, *ACS Photonics*, 2017, **4**, 1539.
142 A. Fernandez-Bravo, K. Yao, E. S. Barnard, N. J. Borys, E. S. Levy, B. Tian, C. A. Tajon, L. Moretti, M. V. Altoe, S. Aloni, K. Beketayev, F. Scotognella, B. E. Cohen,

Open Access Article. Published on 10 2023. Downloaded on 2024/9/11 7:21:17.
This article is licensed under a Creative Commons Attribution-NonCommercial 3.0 Unported Licence.

E. M. Chan and P. J. Schuck, *Nat. Nanotechnol.*, 2018, **13**, 572.
143 L. Jin, Y. Wu, Y. Wang, S. Liu, Y. Zhang, Z. Li, X. Chen, W. Zhang, S. Xiao and Q. Song, *Adv. Mater.*, 2019, **31**, 1807079.
144 Y. Liu, Y. Lu, X. Yang, X. Zheng, S. Wen, F. Wang, X. Vidal, J. Zhao, D. Liu, Z. Zhou, C. Ma, J. Zhou, J. A. Piper, P. Xi and D. Jin, *Nature*, 2017, **543**, 229.
145 X. Peng, B. Huang, R. Pu, H. Liu, T. Zhang, J. Widengren, Q. Zhan and H. Ågren, *Nanoscale*, 2019, **11**, 1563.
146 C. Chen, B. Liu, Y. Liu, J. Liao, X. Shan, F. Wang and D. Jin, *Adv. Mater.*, 2021, **33**, 2008847.
147 H. Dong, L.-D. Sun and C.-H. Yan, *Front. Chem.*, 2021, **8**, 619377.
148 C. Chen, L. Ding, B. Liu, Z. Du, Y. Liu, Xi. Di, X. Shan, C. Lin, M. Zhang, X. Xu, X. Zhong, J. Wang, L. Chang, B. Halkon, X. Chen, F. Cheng and F. Wang, *Nano Lett.*, 2022, **22**, 7136.
149 D. Jaque and F. Vetrone, *Nanoscale*, 2012, **4**, 4301.
150 F. Vetrone, R. Naccache, A. Zamarrón, A. J. de la Fuente, F. Sanz-Rodríguez, L. M. Maestro, E. Martin Rodriguez, D. Jaque, J. G. Sole and J. A. Capobianco, *ACS Nano*, 2010, **4**, 3254.
151 E. M. Rodrigues, D. A. Gálico, I. O. Mazali and F. A. Sigoli, *Sens. Actuators, A*, 2019, **291**, 1.
152 C. Hazra, A. Skripka, S. J. L. Ribeiro and F. Vetrone, *Adv. Opt. Mater.*, 2020, **8**, 2001178.
153 C. Krishnaraj, H. Rijckaert, H. S. Jena, P. Van Der Voort and A. M. Kaczmarek, *ACS Appl. Mater. Interfaces*, 2021, **13**, 47010.
154 O. A. Savchuk, J. J. Carvajal, C. D. S. Brites, L. D. Carlos, M. Aguilo and F. Diaz, *Nanoscale*, 2018, **10**, 6602.
155 M. Runowski, N. Stopikowska, D. Szeremeta, S. Goderski, M. Skwierczyńska and S. Lis, *ACS Appl. Mater. Interfaces*, 2019, **11**, 13389.
156 C. D. S. Brites, X. Xie, M. L. Debasu, X. Qin, R. Chen, W. Huang, J. Rocha, X. Liu and L. D. Carlos, *Nat. Nanotechnol.*, 2016, **11**, 851.
157 E. M. Rodrigues, D. A. Gálico, M. A. Lemes, J. Bettini, E. T. Neto, I. O. Mazali, M. Murugesu and F. A. Sigoli, *New J. Chem.*, 2018, **42**, 13393.
158 E. M. Rodrigues, D. A. Gálico, I. O. Mazali and F. A. Sigoli, *Methods Appl. Fluoresc.*, 2017, **5**, 024012.
159 H. Suo, Q. Zhu, X. Zhang, B. Chen, J. Chen and F. Wang, *Mater. Phys. Today*, 2021, **21**, 100520.
160 T. Sun, B. Xu, B. Chen, X. Chen, M. Li, P. Shi and F. Wang, *Nanoscale*, 2017, **9**, 2701.
161 X. Liu, Y. Wang, X. Li, Z. Yi, R. Deng, L. Liang, X. Xie, D. T. B. Loong, S. Song, D. Fan, A. H. All, H. Zhang, L. Huang and X. Liu, *Nat. Commun.*, 2017, **8**, 899.
162 S. Liu, L. Yan, Q. Li, J. Huang, L. Tao and B. Zhou, *Chem. Eng. J.*, 2020, **397**, 125451.
163 R. Huang, S. Liu, J. Huang, H. Liu, Z. Hu, L. Tao and B. Zhou, *Nanoscale*, 2021, **13**, 4812.
164 B. Golesorkhi, S. Naseri, L. Guenee, I. Taarit, F. Alves, H. Nozary and C. Piguet, *J. Am. Chem. Soc.*, 2021, **143**, 15326.
165 Y. Suffren, B. Golesorkhi, D. Zare, L. Guénée, H. Nozary, S. V. Eliseeva, S. Petoud, A. Hauser and C. Piguet, *Inorg. Chem.*, 2016, **55**, 9964.
166 B. Golesorkhi, H. Nozary, A. Fürstenberg and C. Piguet, *Mater. Horiz.*, 2020, **7**, 1279.
167 B. Golesorkhi, A. Fürstenberg, H. Nozary and C. Piguet, *Chem. Sci.*, 2019, **10**, 6876.
168 N. Souri, P. Tian, C. Platas-Iglesias, K.-L. Wong, A. Nonat and L. J. Charbonnière, *J. Am. Chem. Soc.*, 2017, **139**, 1456.
169 A. Nonat, S. Bahamyirou, A. Lecointre, F. Przybilla, Y. Mély, C. Platas-Iglesias, F. Camerel, O. Jeannin and L. J. Charbonnière, *J. Am. Chem. Soc.*, 2019, **141**, 1568.
170 A. M. Nonat and L. J. Charbonnière, *Coord. Chem. Rev.*, 2020, **409**, 213192.
171 M. Kaiser, C. Würth, M. Kraft, I. Hyppänen, T. Soukka and U. Resch-Genger, *Nanoscale*, 2017, **9**, 10051.
172 C. Homann, L. Krukewitt, F. Frenzel, B. Grauel, C. Würth, U. Resch-Genger and M. Haase, *Angew. Chem., Int. Ed.*, 2018, **57**, 8765.
173 C. Würth, S. Fischer, B. Grauel, A. P. Alivisatos and U. Resch-Genger, *J. Am. Chem. Soc.*, 2018, **140**, 4922.
174 R.-G. Xiong, J.-L. Zuo, Z. Yu, X.-Z. You and W. Chen, *Inorg. Chem. Commun.*, 1999, **2**, 490.
175 J.-C. G. Bünzli and S. V. Eliseeva, *J. Rare Earths*, 2010, **28**, 824.
176 G. Xu, Z.-M. Wang, Z. He, Z. Lü, C.-S. Liao and C.-H. Yan, *Inorg. Chem.*, 2002, **41**, 6802.
177 S. A. Junior, F. V. de Almeida, G. F. de Sá and C. M. Donegá, *J. Lumin.*, 1997, **72**, 478.
178 D. A. Gálico, I. O. Mazali and F. A. Sigoli, *J. Lumin.*, 2017, **192**, 224.
179 K. Manseki, Y. Hasegawa, Y. Wada, H. Ichida, Y. Kanematsu and T. Kushida, *J. Lumin.*, 2007, **122**, 262.
180 S. Omagari, T. Nakanishi, T. Seki, Y. Kitagawa, Y. Takahata, K. Fushimi, H. Ito and Y. Hasegawa, *J. Phys. Chem. A*, 2015, **119**, 1943.
181 K. Sheng, W.-D. Si, R. Wang, W.-Z. Wang, J. Dou, Z.-Y. Gao, L.-K. Wang, C.-H. Tung and D. Sun, *Chem. Mater.*, 2022, **34**, 4186.
182 D. T. Thielemann, A. T. Wagner, E. Rösch, D. K. Kölmel, J. G. Heck, B. Rudat, M. Neumaier, C. Feldmann, U. Schepers, S. Bräse and P. W. Roesky, *J. Am. Chem. Soc.*, 2013, **135**, 7454.
183 S. Petit, F. Baril-Robert, G. Pilet, C. Reber and D. Luneau, *Dalton Trans.*, 2009, **34**, 6809.
184 X.-Y. Chen, X. Yang and B. J. Holliday, *Inorg. Chem.*, 2010, **49**, 2583.
185 S. Comby, R. Scopelliti, D. Imbert, L. Charbonnière, R. Ziessel and J.-C. G. Bünzli, *Inorg. Chem.*, 2006, **45**, 3158.
186 F. Baril-Robert, S. Petit, G. Pilet, G. Chastanet, C. Reber and D. Luneau, *Inorg. Chem.*, 2010, **49**, 10970.
187 D. I. Alexandropoulos, S. Mukherjee, C. Papatriantafyllopoulou, C. P. Raptopoulou, V. Psycharis, V. Bekiari, G. Christou and T. C. Stamatatos, *Inorg. Chem.*, 2011, **50**, 11276.
188 S. Omagari, T. Nakanishi, Y. Kitagawa, T. Seki, K. Fushimi, H. Ito, A. Meijerink and Y. Hasegawa, *Sci. Rep.*, 2016, **6**, 1.

© 2023 The Author(s). Published by the Royal Society of Chemistry

Open Access Article. Published on 10 2023. Downloaded on 2024/9/11 7:21:17.
This article is licensed under a Creative Commons Attribution-NonCommercial 3.0 Unported Licence.

189 S. Omagari, T. Nakanishi, Y. Kitagawa, T. Seki, K. Fushimi, H. Ito, A. Meijerink and Y. Hasegawa, *J. Lumin.*, 2018, **201**, 170.
190 X.-L. Li, L.-F. He, X.-L. Feng, Y. Song, M. Hu, L.-F. Han, X.-J. Zheng, Z.-H. Zhang and S.-M. Fang, *CrystEngComm*, 2011, **13**, 3643.
191 D. Shi, X. Yang, Y. Ma, M. Niu and R. A. Jones, *Inorg. Chem.*, 2020, **59**, 14626.
192 W. Hao, X. Yang, Y. Ma, M. Niu, D. Shi and D. Schipper, *Dalton Trans.*, 2021, **50**, 5865.
193 Y. Ma, X. Yang, M. Niu, D. Shi and D. Schipper, *J. Lumin.*, 2022, **241**, 118494.
194 Y. Ma, X. Yang, D. Shi, M. Niu and D. Schipper, *Inorg. Chem.*, 2020, **59**, 17608.
195 Y. Ma, X. Yang, Z. Xiao, X. Liu, D. Shi, M. Niu and D. Schipper, *Chem. Commun.*, 2021, **57**, 7316.
196 W. -Q. Lin, X. -F. Liao, J. -H. Jia, J. -D. Leng, J. -L. Liu, F. -S. Guo and M. -L. Tong, *Chem.–Eur. J.*, 2013, **19**, 12254.
197 D. Shi, X. Yang, H. Chen, D. Jiang, J. Liu, Y. Ma, D. Schipper and R. A. Jones, *Chem. Commun.*, 2019, **55**, 13116.
198 D. Shi, X. Yang, H. Chen, Y. Ma, D. Schipper and R. A. Jones, *J. Mater. Chem. C*, 2019, **7**, 13425.
199 T. L. King, O. E. Palomero, A. B. Bard, J. A. Espinoza Jr, H. Guo, D. Schipper, X. Yang, L. J. DePue, E. L. Que and R. A. Jones, *J. Coord. Chem.*, 2021, **74**, 92.
200 X.-Y. Li, Y. Jing, J. Zheng, H. Ding, Q. Li, M.-H. Yu and X.-H. Bu, *Cryst. Growth Des.*, 2020, **20**, 5294.
201 D. Guettas, C. M. Balogh, C. Sonneville, Y. Malicet, F. Lepoivre, E. Onal, A. Fateeva, C. Reber, D. Luneau, O. Maury and G. Pilet, *Eur. J. Inorg. Chem.*, 2016, **2016**, 3932.
202 R. C. Knighton, L. K. Soro, A. Lecointre, G. Pilet, A. Fateeva, L. Pontille, L. Francés-Soriano, N. Hildebrandt and L. J. Charbonniere, *Chem. Commun.*, 2021, **57**, 53.
203 R. C. Knighton, L. K. Soro, L. Francés-Soriano, A. Rodríguez-Rodríguez, G. Pilet, M. Lenertz, C. Platas-Iglesias, N. Hildebrandt and L. J. Charbonniere, *Angew. Chem., Int. Ed.*, 2022, **61**, e202113114.
204 A. N. C. Neto, E. Mamontova, A. M. P. Botas, C. D. S. Brites, R. A. S. Ferreira, J. Rouquette, Y. Guari, J. Larionova, J. Long and L. D. Carlos, *Adv. Opt. Mater.*, 2022, **10**, 2101870.
205 C. Krishnaraj, H. Rijckaert, H. S. Jena, P. Van Der Voort and A. M. Kaczmarek, *ACS Appl. Mater. Interfaces*, 2021, **13**, 47010.
206 A. M. Kaczmarek, Y.-Y. Liu, M. K. Kaczmarek, H. Liu, F. Artizzu, L. D. Carlos and P. van Der Voort, *Angew. Chem., Int. Ed.*, 2020, **132**, 1948.
207 A. Cadiau, C. D. S. Brites, P. M. J. Costa, R. A. S. Ferreira, J. Rocha and L. D. Carlos, *ACS Nano*, 2013, **7**, 7213.
208 V. Trannoy, A. N. Carneiro Neto, C. D. S. Brites, L. D. Carlos and H. Serier-Brault, *Adv. Opt. Mater.*, 2021, **9**, 2001938.
209 K. Karachousos-Spiliotakopoulos, V. Tangoulis, N. Panagiotou, A. Tasiopoulos, E. Moreno-Pineda, W. Wernsdorfer, M. Schulze, A. M. P. Botas and L. D. Carlos, *Dalton Trans.*, 2022, **51**, 8208.
210 R. A. S. Ferreira, E. Mamontova, A. M. P. Botas, M. Shestakov, J. Vanacken, V. Moshchalkov, Y. Guari, L. F. Chibotaru, D. Luneau, P. S. André, J. Larionova, J. Long and L. D. Carlos, *Adv. Opt. Mater.*, 2021, **9**, 2101495.
211 J. Wang, J. J. Zakrzewski, M. Heczko, M. Zychowicz, K. Nakagawa, K. Nakabayashi, B. Sieklucka, S. Chorazy and S.-I. Ohkoshi, *J. Am. Chem. Soc.*, 2020, **142**, 3970.
212 D. M. Lyubov, A. N. Carneiro Neto, A. Fayoumi, K. A. Lyssenko, V. M. Korshunov, I. V. Taydakov, F. Salles, Y. Guari, J. Larionova, L. D Carlos, J. Long and A. A. Trifonov, *J. Mater. Chem. C*, 2022, **10**, 7176.
213 D. A. Gálico, I. O. Mazali and F. A. Sigoli, *New J. Chem.*, 2018, **42**, 18541.
214 D. A. Gálico, I. O. Mazali and F. A. Sigoli, *Int. J. Mol. Sci.*, 2022, **23**, 14526.
215 A. A. Kitos, D. A. Gálico, R. Castañeda, J. S. Ovens, M. Murugesu and J. Brusso, *Inorg. Chem.*, 2020, **59**, 11061.
216 A. A. Kitos, D. A. Gálico, N. Mavragani, R. Castañeda, J. O. Moilanen, J. L. Brusso and M. Murugesu, *Chem. Commun.*, 2021, **57**, 7818.
217 X.-Q. Guo, L.-P. Zhou, L.-X. Cai and Q.-F. Sun, *Chem.–Eur. J.*, 2018, **24**, 6936.
218 P. G. Derakhshandeh, S. Abednatanzi, L. Bourda, S. Dalapati, A. Abalymov, M. Meledina, Y.-Y. Liu, A. G. Skirtach, K. Van Hecke, A. M. Kaczmarek and P. Van Der Voort, *J. Mater. Chem. C*, 2021, **9**, 6436.
219 R. Marin, D. A. Gálico, R. Gayfullina, J. O. Moilanen, L. D. Carlos, D. Jaque and M. Murugesu, *J. Mater. Chem. C*, 2022, **10**, 13953.
220 A. Pilch, C. Würth, M. Kaiser, D. Wawrzyńczyk, M. Kurnatowska, S. Arabasz, K. Prorok, M. Samoć, W. Strek, U. Resch-Genger and A. Bednarkiewicz, *Small*, 2017, **20**, 1701635.
221 A. Pilch, D. Wawrzyńczyk, M. Kurnatowska, B. Czaban, M. Samoć, W. Strek and A. Bednarkiewicz, *J. Lumin.*, 2017, **182**, 114.
222 R. Naccache, F. Vetrone, V. Mahalingam, L. A. Cuccia and J. A. Capobianco, *Chem. Mater.*, 2009, **21**, 717.
223 P. Tadge, R. S. Yadav, P. K. Vishwakarma, S. B. Rai, T.-M. Chen, S. Sapra and S. Ray, *J. Alloys Compd.*, 2020, **821**, 153230.
224 R. Joshi, S. Patra, M. Srivastava, B. P. Singh, A. Chakraborty, S. B. Shelar, R. Chakravarty, S. Chakraborty and R. S. Ningthoujam, *ACS Appl. Nano Mater.*, 2022, **5**, 12962.